review, see Kong et al.[16]). Intriguingly, it has been shown that Nrf2 is prevented from accessing the nucleus through tethering to an inhibitor protein, Kelch-like ECH-associated protein 1 (Keap1).[17,18] Recent work has shown that the inhibitory mechanism is probably via the ability of Keap1 to direct Nrf2 for proteosome-mediated degradation under conditions of normal cellular homeostasis.[19-21] Although the triggering mechanism for the uncoupling event is not known, it has been postulated to depend on 1 or more reactive thiol groups in the Keap1 molecule.[17] Since all ARE inducers react with sulfhydryl groups, it has been suggested that Keap1 could be a candidate cellular xenobiotic sensor/trigger.[22]

Acetaminophen (paracetamol) is a human hepatotoxin at high doses and is still associated with several hundred deaths a year in both the United States[23] and the United Kingdom.[24] At therapeutic doses, toxicity is an extremely rare event. Despite over 30 years of research into its mechanism of toxicity, the precise biochemical basis remains unknown.[25] The role of metabolic activation in acetaminophen hepatotoxicity has been confirmed by studies with cytochrome P450 knockout mice,[26,27] and it has been proposed that an electrophilic species, N-acetyl-*p*-benzoquinoneimine (NAPQI), underlies the tissue damage observed. NAPQI can react directly with protein and nonprotein thiols, and GSH depletion is a hallmark of acetaminophen poisoning.[28] This process occurs remarkably rapidly with protein adducts being detectable in mouse liver within 15 minutes of an intraperitoneal (IP) dose of acetaminophen.[29] Furthermore, the formation of NAPQI may be associated with the generation of ROS and oxidative stress, and this has been suggested as a primary cause of the liver damage,[30-32] although several other mechanisms have also been implicated. Depressed mitochondrial function aggravated by the formation of peroxynitrite from superoxide and nitric oxide, together with disrupted calcium homeostasis are also believed to be involved in acetaminophen-induced liver injury (for reviews, see Cohen et al.[31] and Jaeschke et al.[32]). Two independent studies with gene knockout mice have shown that acetaminophen hepatotoxicity is exacerbated in the absence of Nrf2,[14,33] suggesting that the antioxidant response is activated by exposure to acetaminophen and affords protection. However, it has not yet been demonstrated whether acetaminophen treatment *in vivo* actually results in Nrf2 activation. Here we report that administration of acetaminophen to mice does indeed result in increased nuclear levels of Nrf2 in the liver, consistent with a pronounced nuclear translocation of Nrf2 from the cytoplasm. Furthermore, we have investigated the functionality of Nrf2 activation by demonstrating increased expression of several downstream Nrf2 target genes.

Materials and Methods

All chemicals were purchased from Sigma (Poole, UK) unless otherwise stated.

Animals were obtained from Charles River (Margate, UK). All experiments were undertaken in accordance with criteria outlined in a license granted under the Animals (Scientific Procedures) Act of 1986 and approved by the Animal Ethics Committee of the University of Liverpool.

Dosing Regime. Nonfasted animals were dosed as described previously.[34] Briefly, male CD-1 mice (25 - 35 g) were administered a single IP dose of acetaminophen (50, 150, 300, 530, 700, and 1000 mg/kg in 0.9% saline), diethyl maleate (DEM; 2.35, 4.7, and 7.05 mmol/kg, administered in corn oil), or buthionine sulfoximine (BSO; 7.2 mmol/kg in 0.9% saline). Untreated animals or animals treated with vehicle alone were used as controls. Various concentrations of acetaminophen in saline (15 mg/mL for the 50 and 150 mg/kg doses and 30 mg/mL for the 300, 530, 700, and 1000 mg/kg doses), DEM in corn oil (0.622 mol for each of the doses) and BSO in saline (1 mol) were prepared. The volumes injected in the acetaminophen studies varied from 100 μL to 1000 μL, and an equal volume of saline was injected into each of the vehicle control groups. For the DEM studies, 100 μL to 300 μL of DEM in corn oil was injected; 100 μL of corn oil was injected into the vehicle control mice. For the BSO study, equal volumes of saline or BSO in saline (approx 200 μL) were injected into the mice. At various time points after dosing, the animals were killed by cervical dislocation and the livers were removed immediately and rinsed in 0.9% saline.

Determination of Serum Alanine Transaminase Levels. Blood was collected 5 hours (acetaminophen treatment) or 24 hours (DEM treatment) after treatment by cardiac puncture from a satellite group of 2 animals (acetaminophen treatment) or 4 animals (DEM treatment) included with each of the doses investigated. The blood was stored at 4°C and allowed to clot overnight prior to isolation of serum. Serum alanine transaminase (ALT) levels were determined using ThermoTrace Infinity ALT Liquid stable reagent (Alpha Labs, Eastleigh, UK), according to the manufacturer's instructions. Hepatotoxicity was considered to be indicated at levels of ALT greater than 200 IU/L, which in our experience are associated with whole organ manifestations of toxicity.

Determination of Hepatic Reduced GSH Levels. Hepatic GSH was determined using a microtiter plate assay according to the method of Vandeputte et al.[35] The GSH levels were calculated by subtracting the amount of glutathione disulfide from the amount of total GSH in each sample.

Nuclear Extractions. Mouse hepatic nuclear protein extractions were carried out on fresh, homogenized tissue, using the classical Dignam procedure, as described previously,[36,37] with the exception of the nuclear extracts prepared from the acetaminophen- and BSO-treated mice used for Western analysis. For these samples, the whole nuclei prepared by the conventional centrifugation steps as outlined in the Dignam method were solubilized at 4°C for 10 minutes in a radio-immunoprecipitation assay (RIPA) buffer (Dignam lysis buffer containing 1% sodium deoxycholate and 0.1% sodium dodecyl sulfate (SDS) (wt/vol)) and centrifuged at 14,000*g* for 10 minutes at 4°C. The supernatants were removed and stored at −80°C prior to analysis. Separate extracts were prepared using the conventional (Dignam) 0.35 mol NaCl nuclear protein extraction for the DEM-treated samples.

Western Analysis. Hepatic Nrf2 nuclear translocation was determined by Western blot analysis. Briefly, nuclear extracts (25 μg of protein) were separated by denaturing electrophoresis on premade 10% or 12% Nupage Novex Bis-Tris gels (Invitrogen, Paisley, UK) using 3-(N-Morpholino) propane sulfonic acid (MOPS)-SDS running buffer and subsequently transferred to nitrocellulose membranes. After incubation in blocking buffer (10% fat-free milk in Tris-buffered saline (TBS, pH 7) containing 1% Tween 20) for 0.5 hours, membranes were incubated with a rabbit anti-Nrf2 antiserum[21] at 1:4000 in TBS-Tween containing 2% milk for 1 hour. To ensure equal loading and transfer in the Western analysis of nuclear extracts, membranes were routinely stained using Ponceau Red. Following multiple washes with TBS-Tween, the secondary antibody was added (peroxidase-conjugated goat anti-rabbit immunoglobulin G; 1:4000 in TBS-Tween containing 2% milk). Visualization of the protein-antibody conjugate was performed using enhanced chemiluminescence, and band volumes were quantified by UVISoft software (UVITech, Cambridge, UK).

Northern Analysis. Heme oxygenase-1 (HO-1), glutamate cysteine ligase catalytic subunit (GCLC), and microsomal epoxide hydrolase (mEH) messenger RNA (mRNA) levels were determined by conventional Northern blot analysis. The 18S ribosomal RNA band was used as the internal control.

Statistical Analysis. Results are expressed as mean ± standard deviation. All values to be compared were analyzed for nonnormality using the Shapiro-Wilk test and for equivalence of variance between groups with the F test. Student's unpaired *t* test was used where parametric analysis was indicated; otherwise, the Mann-Whitney test was used. Results were considered significant when *P* values were less than .05.

Results

***Acetaminophen Administration Triggers Nrf2 Nuclear Translocation* In Vivo.** Activation of Nrf2 was determined by Western analysis of nuclear extracts from liver homogenate prepared from CD-1 mice treated with a range of acetaminophen doses. Acetaminophen resulted in a pronounced increase in nuclear Nrf2, consistent with enhanced nuclear translocation. Ideally, this translocation would be monitored as the appearance of the Nrf2 protein in the nuclei concomitant with a decrease in the protein in the cytosol. In fact, we were unable to detect Nrf2 in liver cytosolic fractions from any of the control or treated animals. This is not unexpected given that Nrf2 is known to be constitutively degraded prior to activation, at which point the protein migrates to the nucleus.[19–21] Furthermore, we have ruled out the possibility that the chemicals tested in this study might interact with the Nrf2 protein to enhance its immunogenicity in our assay by incubating rNrf2 with NAPQI (the reactive metabolite of acetaminophen) and DEM *in vitro*: the Nrf2 signal did not change after treatment (data not shown). Fig. 1A shows a representative Western blot of nuclear extracts obtained from animals treated with 700 mg/kg acetaminophen and vehicle controls. The induced Nrf2 protein is identified in the treated nuclei by the inclusion of a co-migrating mouse Nrf2 positive control. Nrf2 positive control was also spiked into several putative Nrf2-induced nuclear extracts to confirm the probable identity of the induced band (data not shown). The nonspecific bands were revealed as abundant liver proteins by the use of Ponceau Red staining. Nrf2 nuclear translocation was observed in each of the 5 treated animals compared to the vehicle-treated controls at and above a dose of 150 mg/kg acetaminophen (Fig. 1B). This occurred at each of the doses within 60 minutes after acetaminophen administration. Only low levels of nuclear Nrf2 were detected in the control animals from any of the treatment groups.

Translocation of Nrf2 was not obviously associated with the toxicity of the acetaminophen dose, at least as assessed by plasma ALT levels (Fig. 1B), where we have assumed hepatotoxicity at ALT values above 200 IU/L in our 5-hour satellite treatment groups. In our experience, ALT levels above 200 IU/L are associated with severe overt toxicity. Nuclear Nrf2 was increased above control levels at both nontoxic and toxic doses, although nuclear Nrf2 levels were highest at the 2 most toxic doses.

To define the relationship between the extent of Nrf2 nuclear translocation and the dose of acetaminophen, we pooled the 5 nuclear extracts obtained at each dose and

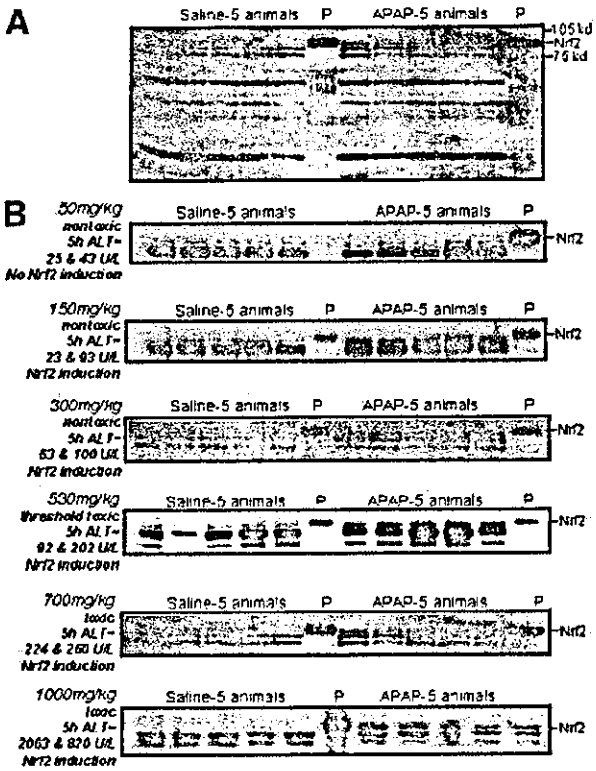

Fig. 1. Acetaminophen induces nuclear translocation of Nrf2 independently of hepatotoxicity. Acetaminophen, or saline vehicle alone, was administered IP to CD-1 mice. After 60 minutes, animals were killed and whole liver nuclei prepared, washed, and extracted. Extracts (25 μg) representing liver nuclear proteins obtained from individual animals were separated by electrophoresis, alongside a mouse Nrf2-transfected 293T cell extract positive control (P) and analyzed by Western blotting. (A) A representative gel showing Nrf2 translocation at 700 mg/kg is shown in full. (B) A close-up image of the gel in the region around the correct migration of Nrf2 is shown at each dose. Each of the analyses was performed at least twice and yielded similar results. The toxicity of each of the doses of acetaminophen is also shown, as assessed by an ALT toxicity assay, carried out on a satellite group of 2 animals per treatment, 5 hours after dosing. APAP, acetaminophen.

subjected these to Western analysis (Fig. 2A). The means of data from 3 separate analyses were then plotted against the treatment dose of acetaminophen. The error bars represent the SD obtained within each of the treatment groups in the analyses shown in Fig. 1B and therefore are representative of the interanimal variation in nuclear Nrf2. The amount of Nrf2 present in the nuclear fraction was found to be linearly associated ($P < .0001$) with the dose of acetaminophen administered, from nontoxic through to toxic doses (Fig. 2B).

***Diethyl Maleate Administration Triggers Nrf2 Nuclear Translocation* In Vivo.** The direct relationship between dose and nuclear Nrf2 obtained with acetaminophen indicated that hepatotoxicity as assessed by ALT determination was not required to cause Nrf2 activation *in vivo*. To confirm this observation, we employed the model compound DEM, which is equally as effective as acetaminophen in depleting GSH but lacks its ability to elicit elevated serum transaminases, indicative of liver damage, at the doses used in this study. Treatment of mice with DEM for 60 minutes resulted in hepatic Nrf2 nuclear translocation (Fig. 3A). This translocation was significantly different from corn oil control values at the 4.7 mmol/kg (236 ± 31% of corn oil controls; $P < .0005$) and 7.05 mmol/kg (652 ± 55% of corn oil controls; $P < .0001$) doses of DEM. No toxicity was seen at any of the doses of DEM used, as judged by the 24-hour ALT data (ALT data: 2.35 mmol/kg = 28 ± 21 U/L; 4.7 mmol/kg = 26 ± 17 U/L; 7.05 mmol/kg = 17 ± 5.7 U/L).

Acetaminophen and Diethyl Maleate Treatment Induces Maximal Nuclear Nrf2 Levels 60 Minutes After Treatment. In order to understand better the nature of the nuclear Nrf2 response to acetaminophen and DEM, we carried out time course studies over a 48-hour period. Both treatments elicited significantly increased levels of nuclear Nrf2 after just 30 minutes (Fig. 4), maximum levels being attained after approximately 1 hour. Thereafter, nuclear Nrf2 levels dropped in both treatments. Nrf2 had returned to control levels between 2 hours and 24 hours after treatment with DEM; this process was slower in the acetaminophen-treated mice, in which baseline levels were reached after approximately 48 hours.

Nrf2 Nuclear Translocation* In Vivo *Is Functionally Relevant as Assessed by Northern Blotting of Nrf2-Dependent Genes. Messenger RNA levels of 3 genes, HO-1, GCLC, and mEH, known to be transcriptionally dependent on Nrf2,[9,10] were analyzed in livers of mice treated with acetaminophen or DEM. At a dose of 530 mg/kg of acetaminophen, at which we observed an approximately 4-fold increase in nuclear Nrf2 (Fig. 2), mRNA levels of *mEH, GCLC,* and *HO-1* were significantly increased 60 minutes after drug administration compared with vehicle-treated controls (Fig. 5A). This confirms that the Nrf2 translocation observed was functionally significant. We also assessed the effect of translocation of Nrf2, at the highest and lowest doses of acetaminophen that affected nuclear accumulation of the bZip protein, on the expression of these genes. Interestingly, at the 150 mg/kg dose, which was the lowest dose that promoted Nrf2 translocation, only the HO-1 mRNA was significantly increased (Fig. 5B). At the 1,000 kg dose, there were no significant differences between the treated and control groups in the mRNA expression of HO-1, GCLC, or mEH (Fig. 5C). We also assessed these genes after administration of 7.05 mmol/kg DEM to check that the effects we observed with acetaminophen were not

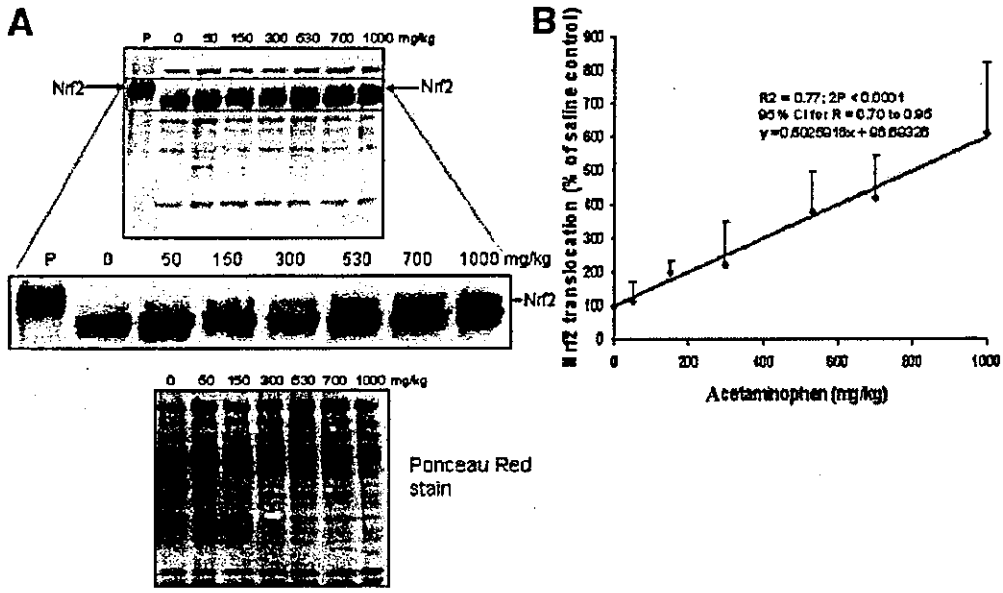

Fig. 2. Acetaminophen induces Nrf2 nuclear translocation *in vivo* in a linear fashion. Acetaminophen, or saline vehicle alone, was administered IP to CD-1 mice. After 60 minutes, animals were killed and whole liver nuclei prepared, washed, and extracted. Extracts (25 μg) were pooled and separated by electrophoresis as described in Fig 1. The analysis was performed 3 times. (A) **(top)** A representative gel is shown. Membranes probed for Nrf2 by Western blotting were always reversibly stained using Ponceau Red stain prior to blocking and antibody probing. This ensured equal loading of total nuclear protein onto each gel and provided a means for monitoring the integrity of the nuclear extracts from each of the treatment groups. A typical stained membrane is shown and is identical to the membrane probed for Nrf2. The staining shows little difference between the treatment groups with respect to the pattern of abundant nuclear proteins detectable using this technique. The gels were densitometrically scanned, and the amount of nuclear Nrf2 was determined as a percentage of the vehicle-treated animals. (B) The means of these determinations were then plotted against the dose of acetaminophen administered. The **error bars** represent the SD of the data (n = 5) for each of the treatment groups as calculated from the densitometry of Nrf2 in each of the nuclear extracts from each group in discrete Western analyses, as shown in Fig. 1B. SD values have been normalized to each of the data points to give an estimate of the interanimal variation within each group.

chemical-specific. In fact, the mRNAs of 2 of these genes, *HO-1* and *GCLC*, were numerically increased upon DEM treatment (Fig. 5D), suggesting that the Nrf2 translocation observed with DEM is also functionally significant.

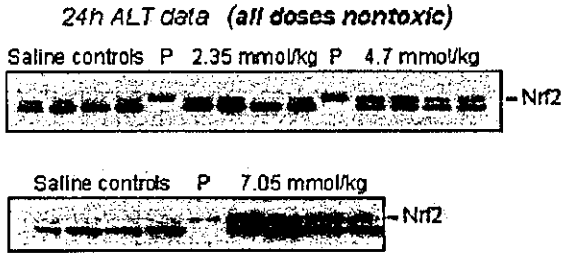

Fig. 3. Nontoxic doses of diethyl maleate (DEM) induce Nrf2 nuclear translocation *in vivo*. DEM, with time-matched controls, was administered IP to CD-1 mice (n = 4 for each dose plus controls). After 60 minutes, animals were killed and whole liver nuclei prepared, washed, and extracted. Extracts (25 μg) representing liver nuclear proteins obtained from individual animals were separated by electrophoresis, alongside a mouse Nrf2-transfected 293T cell extract positive control (P), and analyzed by Western blotting. The analyses were performed twice, and representative gels are shown here. The gels were densitometrically scanned, and the amount of nuclear Nrf2 was determined as a percentage of the time-matched control animals.

Translocation of Nrf2 to the Nucleus Is Associated With Levels of Hepatic GSH but Also Requires Chemical Modification of Sensor Protein(s). Since both acetaminophen and DEM are known to deplete GSH, the primary antioxidant in the liver, the relationship between hepatic GSH and Nrf2 nuclear translocation was investigated. We measured hepatic GSH at each of the doses of acetaminophen and DEM used to investigate translocation, 60 minutes after administration. Fig. 6A shows that nuclear Nrf2 translocation may be associated with GSH for both acetaminophen and DEM treatment; however, the nature of the relationship appears to be nonlinear.

The relationship between Nrf2 nuclear translocation and GSH depletion was also expressed relative to the dose of acetaminophen administered. As shown in Fig. 6B, a small increase in Nrf2 translocation is seen when GSH is depleted to 30% of its initial level. This increase is much more dramatic when GSH falls below 30%.

Finally, the association between Nrf2 activation and GSH levels was further investigated using another GSH-depleting agent, BSO. BSO inhibits GCLC, the rate-limiting enzyme in GSH synthesis, leading to a fall in hepatic GSH, but it does not possess the α,β-unsaturated ketone

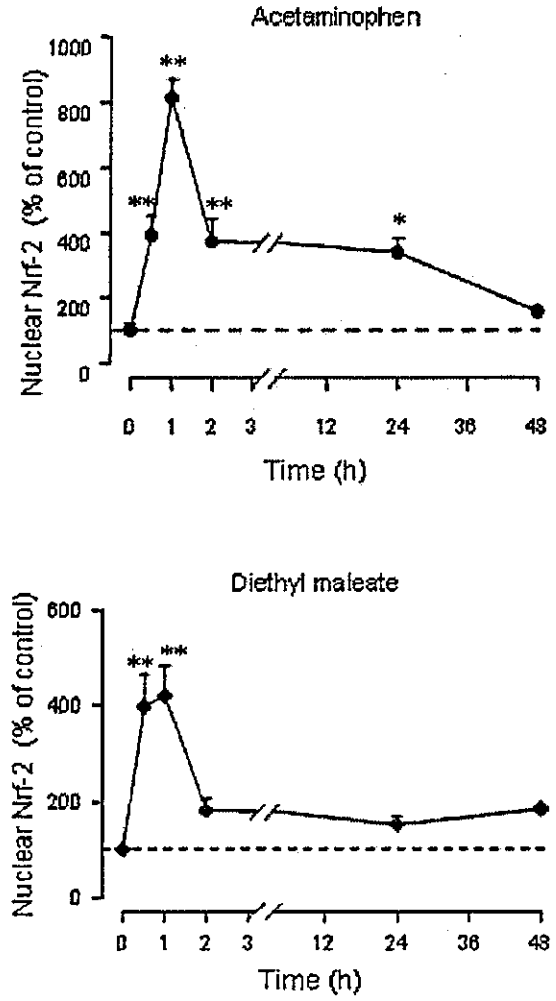

Fig. 4. Acetaminophen and diethyl maleate (DEM) treatment *in vivo* elicits enhanced hepatic nuclear Nrf2 within 30 minutes. Acetaminophen (530mg/kg in saline) and DEM (4.7 mmol/kg in corn oil) were administered IP to CD-1 mice (n = 3 or 4 for each time point). After the time points indicated, the animals were killed and whole liver nuclei prepared, washed, and extracted. Extracts (25 μg) representing liver nuclear proteins obtained from individual animals were separated by electrophoresis and analyzed by Western blotting. Each analysis was performed twice. Membranes were routinely verified for equal sample loading and equal transfer efficiency by using Ponceau Red staining. In all cases, values are the means ± SD of a representative experiment from duplicate determinations. For all data, values are expressed as a percentage of the zero time-point control value, indicated by the **broken line**. Statistical significance was assigned relative to untreated control animals as defined in Materials and Methods. $^{*}P < .05$; $^{**}P < .01$.

motif characteristic of a functional Michael acceptor, and is thus unable to modify proteins chemically, as is the case for acetaminophen and DEM. Treatment of mice (n = 5) with BSO for 1 and 2 hours resulted in 60% and 56% depletion in hepatic GSH, respectively. When we assayed levels of hepatic nuclear translocation of Nrf2 in these animals, no increase in either of the sets of BSO-treated animals was observed compared to the time-matched control group (data not shown). It therefore appears that, although Nrf2 activation is probably associated with GSH depletion, this alone is insufficient to trigger the event.

Discussion

The central and critical role played by Nrf2 in coordinating the mammalian cellular defense response to a variety of noxious and potentially harmful stimuli has become increasing well established over the last 10 years. It is now widely accepted that the redox sensitive regulation of this bZip transcription factor represents a convergence point for multiple stress-activated signaling pathways and results in the coordinated up-regulation of a battery of antioxidant proteins involved in cellular defense.[2,38] The involvement of Nrf2 in defense against chemical-induced stress is largely based on *in vitro* studies in cell lines, in which nuclear translocation has been clearly demonstrated following exposure to a variety of chemicals, including tertiary butyl hydroquinone,[39] butylated hydroxy anisole,[40] and DEM,[41] though not to acetaminophen. In contrast, there is a paucity of data demonstrating chemically induced Nrf2 activation *in vivo*. To our knowledge, the only documented evidence for Nrf2 translocation *in vivo* is that describing mouse hepatic nuclear Nrf2 after treatment with 3H-1,2-dithiole-3-thione[42] and a related compound, oltipraz.[43] Thus, the clear demonstration in the current study that acetaminophen administration to mice elicits a pronounced elevation of nuclear Nrf2 levels represents direct evidence for such activation in either an *in vivo* or an *in vitro* model system. Moreover, these data indicate that the nuclear translocation of Nrf2 *in vivo* is associated with levels of GSH, and thus the redox status, but is also dependent on the presence of chemical species with inherent protein reactivity. This follows from the observation that although acetaminophen, DEM, and BSO all depleted GSH to a similar extent, only DEM (a Michael acceptor) and acetaminophen (which is converted to the Michael acceptor NAPQI) elicited a rise in nuclear Nrf2.

The functional significance of the rise in nuclear Nrf2 was investigated by Northern analysis of 3 unrelated genes that have previously been characterized as downstream targets for Nrf2. Transcription of all 3 genes, HO-1, *GCLC*, and *mEH*, was enhanced in line with Nrf2 activation; however, there appeared to be different threshold levels of nuclear Nrf2 required for transcriptional activation in each case. Thus, there was a hierarchical order of induction, with *HO-1* being the only gene induced at the nontoxic 150 mg/kg dose, while all 3 genes were induced

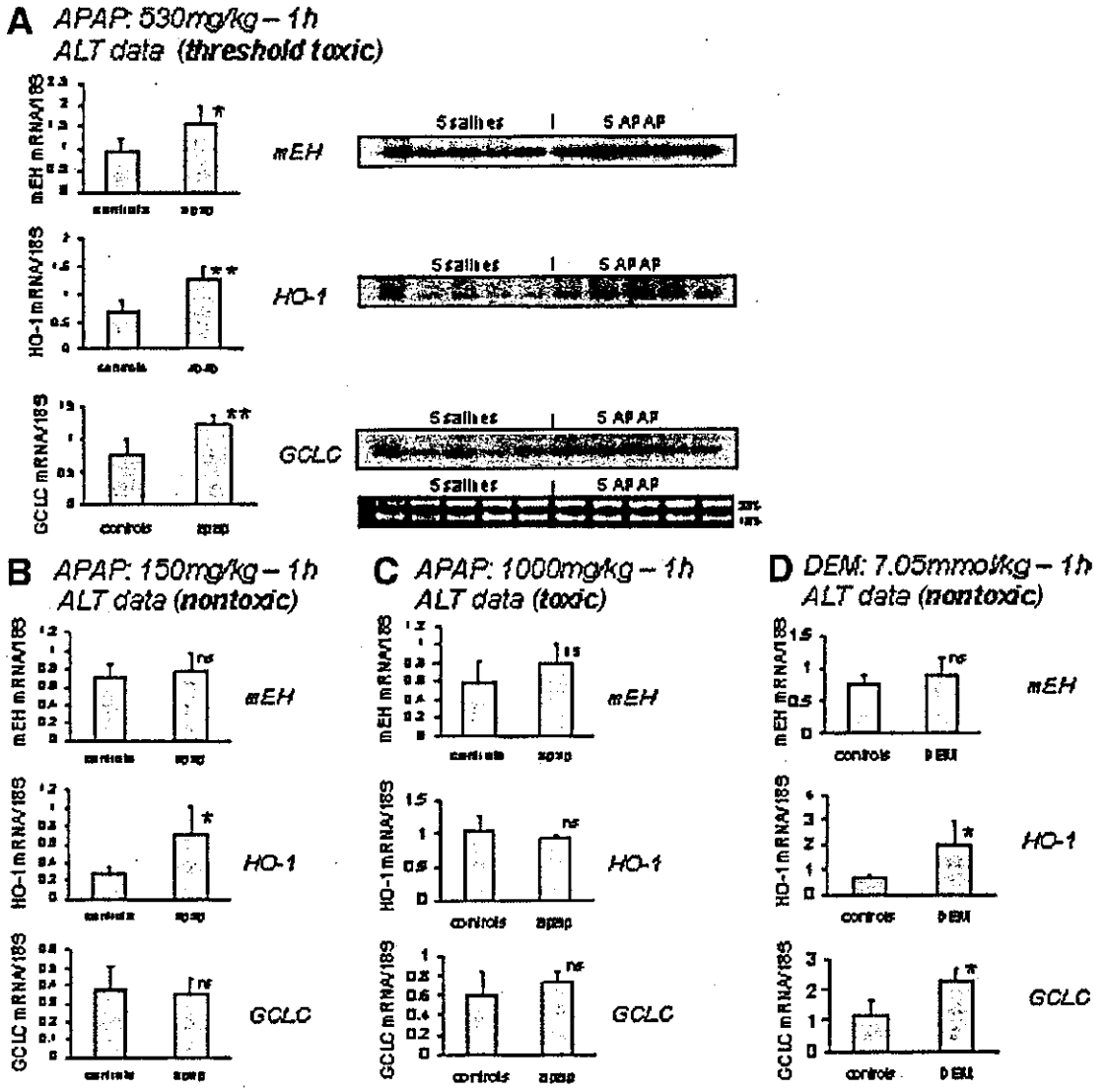

Fig. 5. Translocation of Nrf2 to the nucleus is functionally relevant as assessed by Northern blotting of Nrf2-dependent genes. Acetaminophen, or saline vehicle alone, and diethyl maleate (DEM), with time-matched controls, were administered IP to CD-1 mice (n = 5). After 60 minutes, animals were killed and the liver was removed and washed. Whole liver RNA was extracted and analyzed using Northern blotting (25 μg of total RNA from each animal), employing gene-specific probes corresponding to mouse mEH, HO-1, and GCLC mRNA sequences. In all cases,values are the means ± SD. For all data, values are standardized against 18S ribosomal RNA. Statistical significance was assigned relative to untreated control animals as defined in Materials and Methods. $^*P < .05$; $^{**}P < .01$; ns, not significant.

at the 530 mg/kg dose, which is a threshold dose for overt liver damage. Interestingly, none of the 3 Nrf2-regulated genes was induced at the highest (1000 mg/kg) dose despite the marked Nrf2 nuclear translocation occurring at this dose. Presumably, the level of toxicity associated with this dose results in such widespread cellular malfunctioning that the machinery involved in gene transcription and mRNA synthesis is itself impaired. In fact, cell death caused by acetaminophen may indicate that the toxic insult has overwhelmed repair mechanisms, such as the Nrf2 response, either by causing irreparable damage to it, or by causing other damage too great for the protective responses to deal with effectively. Differential induction of the 3 target genes was also observed with the single, high (7 mmol/kg) but nontoxic, dose of DEM used in this study, at which HO-1 and GCLC were both significantly up-regulated while mEH was unchanged. Thus, it appears that certain genes are more sensitive than others to Nrf2 activation and are induced at lower Nrf2 nuclear levels. Alternatively, since Nrf2 acts as a heterodimer to

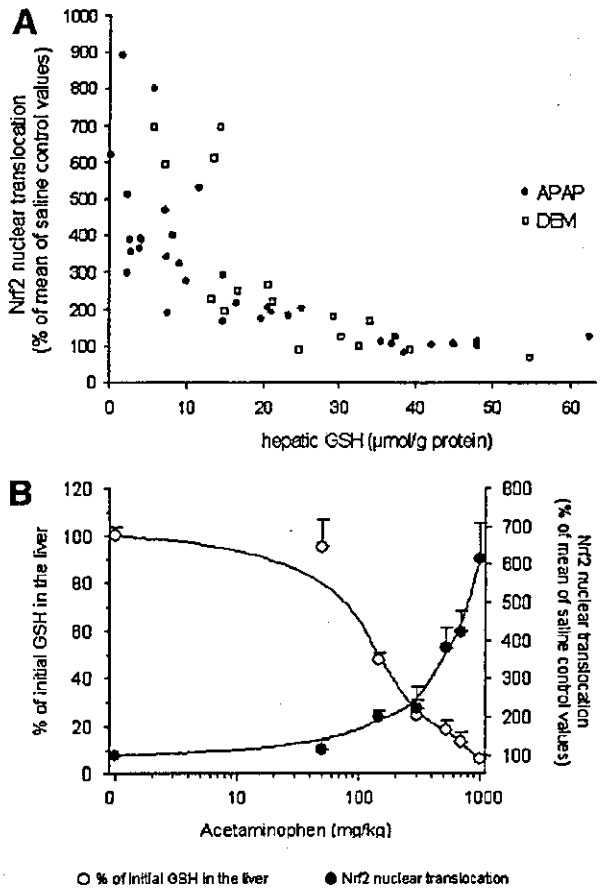

Fig. 6. Nrf2 nuclear translocation is associated with levels of hepatic glutathione (GSH). Acetaminophen, or saline vehicle alone, and diethyl maleate (DEM), with time-matched controls, were administered IP to CD-1 mice. After 60 minutes, animals were killed and the liver was removed and washed. (A) Hepatic GSH levels were determined and plotted against Nrf2 translocation. (B) GSH depletion and Nrf2 translocation were also expressed relative to the dose of acetaminophen. Data are expressed as the mean ± SD, where n = 5.

activate gene transcription, the differential induction of target genes observed may reflect their different preferences with respect to alternative dimerization partners. Precise characterization of the transcription factors recruited by variant forms of the ARE may be required in order to elucidate and define the hierarchical order of Nrf2 target gene transcription.

The linear response in Nrf2 translocation seen at the different doses of acetaminophen contrasts with the nonlinear response in Nrf2 when it is related to GSH. As GSH is depleted to approximately 30% of control levels, a modest increase in Nrf2 translocation is observed up to ≈200% of nuclear control levels (Figs. 6A and B). As GSH drops further, much more pronounced rises are seen in nuclear Nrf2. One could envisage a scenario in which depletion of GSH leads to increasing numbers of the reactive cysteine residues in the cytosolic Nrf2 inhibitor Keap1[22] becoming available to be oxidized or covalently modified (by the DEM molecule itself, or in the case of acetaminophen, by its reactive metabolite, NAPQI). In fact, the relationship we observe between Nrf2 translocation and GSH depletion is very similar to the relationship between hepatic covalent binding and GSH depletion upon administration of acetaminophen first observed by Mitchell et al.[44] This may be supportive of the notion that covalent binding (possibly of Keap1) via Michael addition is the precursor to Nrf2 activation *in vivo*, although a large number of cellular proteins that are adducted by acetaminophen have been identified[45]; it is also possible that the modification of 1 or more of these may play a role in triggering Nrf2 activation or other protective responses. Recent evidence suggests that there are 4 highly reactive cysteines within Keap1.[46] These are located in the intervening region between the 2 protein-binding domains of Keap1; this increases the likelihood that they may be available to act as sensors. The modification of some or all of these residues would lead to steadily increasing numbers of Nrf2 molecules translocating to the nucleus. At a certain threshold, further oxidation/modification of Keap1 may lead to substantial loss of association with Nrf2, enabling a wide-scale nuclear translocation. Whether Keap1 thiol modification occurs directly, possibly through Michael addition, or indirectly through preceding activation of upstream enzymes, is still unresolved. Recent investigations of the induction of GCLC by indomethacin and related indole compounds point to a role for NADPH (MTHFR; 5,10-methylenetetrahydrofolate reductase) oxidase in Keap1 thiol oxidation, through generation of the superoxide anion.[47] Although the universality of this mechanism needs to be clarified, formation of reactive oxygen species, including superoxide, has previously been postulated to be a consequence of acetaminophen metabolism,[32] and this may represent a further mechanism for Nrf2 activation. Evidence for a physiologically based mechanism for Nrf2 activation via covalent modification through Michael addition has recently emerged through studies on the prostaglandin J2 family of anti-inflammatory mediators.[48] These cyclopentenone compounds are dehydration products of prostaglandin D2, and as such contain the α,β-unsaturated ketone motif characteristic of Michael acceptors. Several of their properties, such as induction of glutathione S-transferases, are consistent with an interaction with the Nrf2 system, and it has recently been shown that they are indeed capable of the covalent modification of the Keap1 protein.[49,50] It is our intention to explore the possibility of direct modification of Keap1 by NAPQI

and DEM, in order to clarify the mechanism of induction observed in the present study.

In conclusion, we have detected dynamic changes in the Nrf2 system *in vivo*, associated with 2 discrete chemical agents. These changes are not dependent on a toxic effect of these agents on the liver but are associated with changes in the hepatic level of reduced GSH and the presence of a chemical species with the potential for covalent modification, with the likely consequent oxidative alterations in cell regulatory and sensor proteins. The induction profile seen with Nrf2-regulated genes following acetaminophen treatment, whereby induction was impaired at very high doses despite the linear increase in nuclear Nrf2, may have therapeutic consequences for the targeting of Nrf2 in chemoprotection. The strategic induction of Nrf2 to boost cellular defense mechanisms may alone provide insufficient protection against some forms of chemical stress without the concomitant maintenance of related cellular functions.

Acknowledgment: The authors thank Sylvia Newby and Phil Roberts for technical assistance and Dr. Nicola Hanrahan for assistance with the glutathione assay.

References

1. Prestera T, Zhang Y, Spencer SR, Wilczak CA, Talalay P. The electrophile counterattack response: protection against neoplasia and toxicity. Adv Enzyme Regul 1993;33:281–296.
2. Hayes JD, McMahon M. Molecular basis for the contribution of the antioxidant responsive element to cancer chemoprevention. Cancer Lett 2001;174:103–113.
3. Friling RS, Bergelson S, Daniel V. Two adjacent AP-1-like binding sites form the electrophile-responsive element of the murine glutathione S-transferase Ya subunit gene. Proc Natl Acad Sci USA 1992;89:668–672.
4. Jaiswal AK. Antioxidant response element. Biochem Pharmacol 1994;48: 439–444.
5. Rushmore TH, Pickett CB. Transcriptional regulation of the rat glutathione S-transferase Ya subunit gene. Characterization of a xenobiotic-responsive element controlling inducible expression by phenolic antioxidants. J Biol Chem 1990;265:14648–14653.
6. Rushmore TH, Morton MR, Pickett CB. The antioxidant responsive element. Activation by oxidative stress and identification of the DNA consensus sequence required for functional activity. J Biol Chem 1991;266: 11632–11639.
7. Andrews NC, Erdjument-Bromage H, Davidson MB, Tempst P, Orkin SH. Erythroid transcription factor NF-E2 is a haematopoietic-specific basic-leucine zipper protein. Nature 1993;362:722–728.
8. Venugopal R, Jaiswal AK. Nrf1 and Nrf2 positively and c-Fos and Fra1 negatively regulate the human antioxidant response element-mediated expression of NAD(P)H:quinone oxidoreductase1 gene. Proc Natl Acad Sci USA 1996;93:14960–14965.
9. Wild AC, Moinova HR, Mulcahy RT. Regulation of gamma-glutamylcysteine synthetase subunit gene expression by the transcription factor Nrf2. J Biol Chem 1999;274:33627–33636.
10. Alam J, Stewart D, Touchard C, Boinapally S, Choi AM, Cook JL. Nrf2, a Cap'n'Collar transcription factor, regulates induction of the heme oxygenase-1 gene. J Biol Chem 1999;274:26071–26078.
11. Jeyapaul J, Jaiswal AK. Nrf2 and c-Jun regulation of antioxidant response element (ARE)-mediated expression and induction of gamma-glutamylcysteine synthetase heavy subunit gene. Biochem Pharmacol 2000;59:1433–1439.
12. Chanas SA, Jiang Q, McMahon M, McWalter GK, McLellan LI, Elcombe CR, et al. Loss of the Nrf2 transcription factor causes a marked reduction in constitutive and inducible expression of the glutathione S-transferase Gsta1, Gsta2, Gstm1, Gstm2, Gstm3 and Gstm4 genes in the livers of male and female mice. Biochem J 2002;365:405–416.
13. Chan K, Kan YW. Nrf2 is essential for protection against acute pulmonary injury in mice. Proc Natl Acad Sci USA 1999;96:12731–12736.
14. Enomoto A, Itoh K, Nagayoshi E, Haruta J, Kimura T, O'Connor T, et al. High sensitivity of Nrf2 knockout mice to acetaminophen hepatotoxicity associated with decreased expression of ARE-regulated drug metabolizing enzymes and antioxidant genes. Toxicol Sci 2001;59:169–177.
15. McMahon M, Itoh K, Yamamoto M, Chanas SA, Henderson CJ, McLellan LI, et al. The Cap'n'Collar basic leucine zipper transcription factor Nrf2 (NF-E2 p45-related factor 2) controls both constitutive and inducible expression of intestinal detoxification and glutathione biosynthetic enzymes. Cancer Res 2001;61:3299–3307.
16. Kong AN, Owuor E, Yu R, Hebbar V, Chen C, Hu R, et al. Induction of xenobiotic enzymes by the map kinase pathway and the antioxidant or electrophile response element (ARE/EpRE). Drug Metab Rev 2001;33: 255–271.
17. Itoh K, Wakabayashi N, Katoh Y, Ishii T, Igarashi K, Engel JD, et al. Keap1 represses nuclear activation of antioxidant responsive elements by Nrf2 through binding to the amino-terminal Neh2 domain. Genes Dev 1999;13:76–86.
18. Wakabayashi N, Itoh K, Wakabayashi J, Motohashi H, Noda S, Takahashi S, et al. Keap1-null mutation leads to postnatal lethality due to constitutive Nrf2 activation. Nat Genet 2003;35:238–245.
19. Itoh K, Wakabayashi N, Katoh Y, Ishii T, O'Connor T, Yamamoto M. Keap1 regulates both cytoplasmic-nuclear shuttling and degradation of Nrf2 in response to electrophiles. Genes Cells 2003;8:379–391.
20. Nguyen T, Sherratt PJ, Huang HC, Yang CS, Pickett CB. Increased protein stability as a mechanism that enhances Nrf2-mediated transcriptional activation of the antioxidant response element. Degradation of Nrf2 by the 26 S proteasome. J Biol Chem 2003;278:4536–4541.
21. McMahon M, Itoh K, Yamamoto M, Hayes JD. Keap1-dependent proteasomal degradation of transcription factor Nrf2 contributes to the negative regulation of antioxidant response element-driven gene expression. J Biol Chem 2003;278:21592–21600.
22. Dinkova-Kostova AT, Massiah MA, Bozak RE, Hicks RJ, Talalay P. Potency of Michael reaction acceptors as inducers of enzymes that protect against carcinogenesis depends on their reactivity with sulfhydryl groups. Proc Natl Acad Sci USA 2001;98:3404–3409.
23. Ostapowicz G, Fontana RJ, Schiodt FV, Larson A, Davern TJ, Han SH, et al. Results of a prospective study of acute liver failure at 17 tertiary care centers in the United States. Ann Intern Med 2002;137:947–954.
24. Fagan E, Wannan G. Reducing paracetamol overdoses. Br Med J 1996; 313:1417–1418.
25. Pierce RH, Franklin CC, Campbell JS, Tonge RP, Chen W, Fausto N, et al. Cell culture model for acetaminophen-induced hepatocyte death in vivo. Biochem Pharmacol 2002;64:413–424.
26. Lee SS, Buters JT, Pineau T, Fernandez-Salguero P, Gonzalez FJ. Role of CYP2E1 in the hepatotoxicity of acetaminophen. J Biol Chem 1996;271: 12063–12067.
27. Zaher H, Buters JT, Ward JM, Bruno MK, Lucas AM, Stern ST, et al. Protection against acetaminophen toxicity in CYP1A2 and CYP2E1 double-null mice. Toxicol Appl Pharmacol 1998;152:193–199.
28. Potter WZ, Thorgeirsson SS, Jollow DJ, Mitchell JR. Acetaminophen-induced hepatic necrosis. V. Correlation of hepatic necrosis, covalent binding and glutathione depletion in hamsters. Pharmacology 1974;12:129–143.
29. Muldrew KL, James LP, Coop L, McCullough SS, Hendrickson HP, Hinson JA, et al. Determination of acetaminophen-protein adducts in mouse liver and serum and human serum after hepatotoxic doses of acetaminophen using high-performance liquid chromatography with electrochemical detection. Drug Metab Dispos 2002;30:446–451.

30. Harman AW. The effectiveness of antioxidants in reducing paracetamol-induced damage subsequent to paracetamol activation. Res Commun Chem Pathol Pharmacol 1985;49:215–228.
31. Cohen SD, Hoivik DJ, Khairallah EA. In: Plaa GL, Hewitt WR, eds. Toxicology of the Liver. Vol. 1. 2nd ed. Washington D.C.: Taylor & Francis; 1998; 159–186.
32. Jaeschke H, Knight TR, Bajt ML. The role of oxidant stress and reactive nitrogen species in acetaminophen hepatotoxicity. Toxicol Lett 2003;144: 279–288.
33. Chan K, Han XD, Kan YW. An important function of Nrf2 in combating oxidative stress: detoxification of acetaminophen. Proc Natl Acad Sci USA 2001;98:4611–4616.
34. Kitteringham NR, Powell H, Clement YN, Dodd CC, Tettey JN, Pirmohamed M, et al. Hepatocellular response to chemical stress in CD-1 mice: induction of early genes and gamma-glutamylcysteine synthetase. HEPATOLOGY 2000;32:321–333.
35. Vandeputte C, Guizon I, Genestie-Denis I, Vannier B, Lorenzon G. A microtiter plate assay for total glutathione and glutathione disulfide contents in cultured/isolated cells: performance study of a new miniaturized protocol. Cell Biol Toxicol 1994;10:415–421.
36. Dignam JD, Lebovitz RM, Roeder RG. Accurate transcription initiation by RNA polymerase II in a soluble extract from isolated mammalian nuclei. Nucleic Acids Res 1983;11:1475–1489.
37. Israel N, Gougerot-Pocidalo MA, Aillet F, Virelizier JL. Redox status of cells influences constitutive or induced NF-kappa B translocation and HIV long terminal repeat activity in human T and monocytic cell lines. J Immunol 1992;149:3386–3393.
38. Nguyen T, Sherratt PJ, Pickett CB. Regulatory mechanisms controlling gene expression mediated by the antioxidant response element. Annu Rev Pharmacol Toxicol 2003;43:233–260.
39. Liu RM, Hu H, Robison TW, Forman HJ. Differential enhancement of gamma-glutamyl transpeptidase and gamma-glutamylcysteine synthetase by tert-butylhydroquinone in rat lung epithelial L2 cells. Am J Respir Cell Mol Biol 1996;14:186–191.
40. Hayes JD, Chanas SA, Henderson CJ, McMahon M, Sun C, Moffat GJ, et al. The Nrf2 transcription factor contributes both to the basal expression of glutathione S-transferases in mouse liver and to their induction by the chemopreventive synthetic antioxidants, butylated hydroxyanisole and ethoxyquin. Biochem Soc Trans 2000;28:33–41.
41. Sekhar KR, Long M, Long J, Xu ZQ, Summar ML, Freeman ML. Alteration of transcriptional and post-transcriptional expression of gamma-glutamylcysteine synthetase by diethyl maleate. Radiat Res 1997;147:592–597.
42. Kwak MK, Itoh K, Yamamoto M, Sutter TR, Kensler TW. Role of transcription factor Nrf2 in the induction of hepatic phase 2 and antioxidative enzymes in vivo by the cancer chemoprotective agent, 3H-1, 2-dimethiole-3-thione. Mol Med 2001;7:135–145.
43. Ramos-Gomez M, Kwak MK, Dolan PM, Itoh K, Yamamoto M, Talalay P, et al. Sensitivity to carcinogenesis is increased and chemoprotective efficacy of enzyme inducers is lost in nrf2 transcription factor-deficient mice. Proc Natl Acad Sci USA 2001;98:3410–3415.
44. Mitchell JR, Jollow DJ, Potter WZ, Gillette JR, Brodie BB. Acetaminophen-induced hepatic necrosis. IV. Protective role of glutathione. J Pharmacol Exp Ther 1973;187:211–217.
45. Qiu Y, Benet LZ, Burlingame AL. Identification of the hepatic protein targets of reactive metabolites of acetaminophen in vivo in mice using two-dimensional gel electrophoresis and mass spectrometry. J Biol Chem 1998;273:17940–17953.
46. Dinkova-Kostova AT, Holtzclaw WD, Cole RN, Itoh K, Wakabayashi N, Katoh Y, et al. Direct evidence that sulfhydryl groups of Keap1 are the sensors regulating induction of phase 2 enzymes that protect against carcinogens and oxidants. Proc Natl Acad Sci USA 2002;99:11908–11913.
47. Sekhar KR, Crooks PA, Sonar VN, Friedman DB, Chan JY, Meredith MJ, et al. NADPH Oxidase Activity Is Essential for Keap1/Nrf2-mediated Induction of GCLC in Response to 2-Indol-3-yl-methylenequinuclidin-3-ols. Cancer Res 2003;63:5636–5645.
48. Shibata T, Kondo M, Osawa T, Shibata N, Kobayashi M, Uchida K. 15-deoxy-delta 12,14-prostaglandin J2. A prostaglandin D2 metabolite generated during inflammatory processes. J Biol Chem 2002;277:10459–10466.
49. Shibata T, Yamada T, Ishii T, Kumazawa S, Nakamura H, Masutani H, et al. Thioredoxin as a molecular target of cyclopentenone prostaglandins. J Biol Chem 2003;278:26046–26054.
50. Levonen AL, Landar A, Ramachandran A, Ceaser EK, Dickinson DA, Zanoni G, et al. Cellular mechanisms of redox cell signaling: role of cysteine modification in controlling antioxidant defenses in response to electrophilic lipid oxidation products. Biochem J 2004;378:373–382.

Nrf2 deficiency causes tooth decolourization due to iron transport disorder in enamel organ

Toru Yanagawa[1], Ken Itoh[1,2], Junya Uwayama[1], Yasuaki Shibata[4], Akira Yamaguchi[4], Tsuneyoshi Sano[5], Tetsuro Ishii[1], Hiroshi Yoshida[1] and Masayuki Yamamoto[1,2,3,*]

[1]*Graduate School of Comprehensive Human Sciences,* [2]*JST-ERATO Environmental Response Project,* [3]*Centre for Tsukuba Advanced Research Alliance, University of Tsukuba, 1-1-1 Tennoudai, Tsukuba 305-8577, Japan*

[4]*Division of Oral Pathology and Bone Metabolism, Department of Developmental and Reconstructive Medicine, Nagasaki University Graduate School of Biomedical Sciences, 1-7-1 Sakamoto, Nagasaki, 852-8588, Japan*

[5]*Department of Oral Anatomy, Showa University School of Dentistry, 1-5-8 Hatanodai, Shinagawa-ku, Tokyo 142-8585, Japan*

Rodents have brownish-yellow incisors whose colour represents their iron content. Iron is deposited into the mature enamel by ameloblasts that outline enamel surface of the teeth. Nrf2 is a basic region-leucine zipper type transcription factor that regulates expression of a range of cytoprotective genes in response to oxidative and xenobiotic stresses. We found that genetically engineered Nrf2-deficient mice show decolourization of the incisors. While incisors of wild-type mice were brownish yellow, incisors of Nrf2-deficient mice were greyish white in colour. Micro X-ray imaging analysis revealed that the iron content in Nrf2-deficient mouse incisors were significantly decreased compared to that of wild-type mice. We found that iron was aberrantly deposited in the papillary layer cells of enamel organ in Nrf2-deficient mouse, suggesting that the iron transport from blood vessels to ameloblasts was disturbed. We also found that ameloblasts of Nrf2-null mouse show degenerative atrophy at the late maturation stage, which gives rise to the loss of iron deposition to the surface of mature enamel. Our results thus demonstrate that the enamel organ of Nrf2-deficient mouse has a reduced iron transport capacity, which results in both the enamel cell degeneration and disturbance of iron deposition on to the enamel surface.

Introduction

The brownish yellow colour of the rodent incisors is due to iron deposition in the enamel surface layer (Halse 1973, 1974; Halse & Selvig 1974; Kallenbach 1970). In the enamel organ of rodents, where the tooth develops, a layer of cells that outline the enamel surface called ameloblasts contain the entire sequence of cell development stages. From the apical end toward the incisal end these stages are classified regionally into presecretory, secretory, transition, and maturation stages. Secretory ameloblasts produce enamel matrix proteins, whereas ameloblasts at the maturation stage act to incorporate iron and deposit it into the surface of the mature enamel, in addition to their fundamental roles in enamel formation.

Communicated by: Shunsuke Ishii

**Correspondence*: E-mail: masi@tara.tsukuba.ac.jp

DOI: 10.1111/j.1365-2443.2004.00753.x

In this unique iron transport system, ferritin functions as a transient iron reservoir in the cell, sequestering iron into the cytoplasmic granules (Karim & Warshawsky 1984). This particle first appears free in the cytoplasm, and then gradually becomes confined to the membrane bound ferritin-containing vesicles with the progression of cell developmental stages. Finally, the iron is secreted from ameloblasts into the enamel surface at the end of maturation, presumably through the process of lysosomal digestion of ferritin (Takano & Ozawa 1981).

Iron is critically involved in a wide variety of cellular events ranging from DNA synthesis to cellular respiration (Cammack *et al.* 1990). However, at the same time, free iron generates highly reactive oxygen species via Fenton chemistry and causes an oxidative stress to cells (Linn 1998). Thus, the cellular iron metabolism should be strictly regulated in the presence of various transport and storage proteins (McCord 1998).

Nrf2 belongs to the CNC transcription factor family which share a characteristic basic domain first identified in the Drosophila cap'n'collar (CNC) protein (Itoh *et al.* 1995; Mohler *et al.* 1991). Nrf2 is essential for the coordinate transcriptional induction of phase II enzymes and anti-oxidant genes via anti-oxidant responsive element (ARE) (Itoh *et al.* 1997; Ishii *et al.* 2000). Furthermore, Nrf2 constitutes a crucial cellular sensor for oxidative stress together with its cytoplasmic repressor Keap1, and mediates a key step in the signalling pathway by a novel Nrf2 nuclear shuttling mechanism (Itoh *et al.* 1999b). Activation of Nrf2 leads to the induction of phase II enzyme and anti-oxidant stress genes in response to various stresses (Ishii *et al.* 2000; Itoh *et al.* 1999a).

Whereas Nrf2-deficient mice (*Nrf2*$^{-/-}$) grow normally and are fertile (Itoh *et al.* 1997), the mice are susceptible to various oxidative stresses including acetaminophen intoxication (Enomoto *et al.* 2001; Chan *et al.* 2001), BHT intoxication (Chan & Kan 1999), chemical carcinogenesis (Ramos-Gomez *et al.* 2001), hyperoxia (Cho *et al.* 2002), and diesel exhaust inhalation (Aoki *et al.* 2001). The *Nrf2*$^{-/-}$ mice are also susceptible to lupus-like autoimmune nephritis (Yoh *et al.* 2001). However, no apparent phenotype has yet been described (Itoh *et al.* 1997; Kuroha *et al.* 1998). In this study, we found that incisors of the *Nrf2*$^{-/-}$ mice are decolourized and become greyish white. The examination of the mechanisms leading to the decolourization in the *Nrf2*$^{-/-}$ mouse revealed that the iron transport is defective in the developing enamel organ of *Nrf2*$^{-/-}$ mice.

Results

Decolourization of the maxillary incisors of *Nrf2*$^{-/-}$ mice

In an attempt to find subtle anatomical changes in the germ line *Nrf2*$^{-/-}$ mice (Itoh *et al.* 1997), we noticed that the incisors of *Nrf2*$^{-/-}$ mice are always greyish white (Fig. 1B), while in contrast, incisors of wild-type and heterozygous mutant (*Nrf2*$^{+/-}$) mice are always brownish yellow (Fig. 1A). In order to examine the decolourization phenotype in more detail, we mated *Nrf2*$^{+/-}$ male with *Nrf2*$^{+/-}$ female mice and examined 50 mice for the relationship between *Nrf2* genotype and the incidence of decolourization by macroscopic examination. Fourteen mice had greyish-white incisors and all of them were homozygous for the *Nrf2* germ line mutation. On the contrary, of the 36 mice with brownish yellow incisors, 26 were *Nrf2* heterozygous and 10 were wild-type. Thus, the penetration of decolourization phenotype in *Nrf2*$^{-/-}$ mice was 100% ($P < 0.001$).

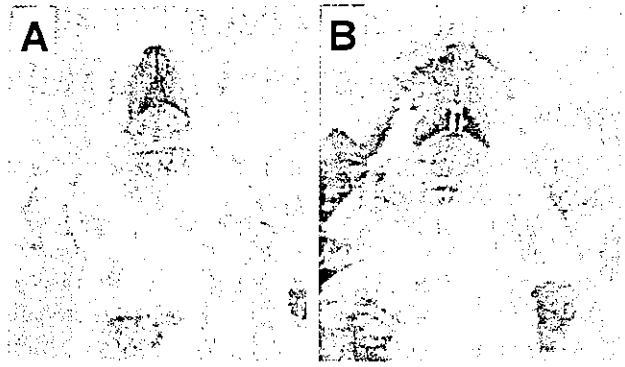

Figure 1 Incisors of *Nrf2*$^{-/-}$ mice are decolourized. The incisors of wild-type mouse show the normal brownish-yellow colour (A), whereas the incisors of *Nrf2*$^{-/-}$ mice have greyish white colour (B).

Iron content in enamel surface was specifically decreased in *Nrf2*$^{-/-}$ mice

Scanning electron microscopic analysis detected no significant structural differences in the tooth surface between wild-type (Fig. 2A) and *Nrf2*$^{-/-}$ mice (Fig. 2D). However, X-ray microanalysis revealed an apparent difference in the iron content on the enamel surfaces between the *Nrf2*$^{-/-}$ and wild-type mice (Table 1). A dot-map image analysis revealed the remarkable decrease of iron content in the enamel surface of *Nrf2*$^{-/-}$ mouse incisors (Fig. 2F) compared to those of wild-type mice (Fig. 2C). Calcium content was within comparable range between wild-type (Fig. 2B) and *Nrf2*$^{-/-}$ mice (Fig. 2E).

Table 1 summarizes the calcium, phosphorus and iron contents of the incisors that were quantified by X-ray microanalysis. Importantly, we found that the mean iron content (Fe% (w/w)) of the *Nrf2*$^{-/-}$ mouse enamel was less than one-tenth of that of the wild-type mouse. The decrease shows gene copy number dependence such that in the *Nrf2*$^{+/-}$ mouse incisors the mean iron content was about one half of that of the wild-type mice. In contrast, no significant difference was observed in the content of calcium and phosphorus amongst *Nrf2*$^{-/-}$, *Nrf2*$^{+/-}$ and wild-type mice. Similarly, the molar ratio (MR) as well as weight percentage ratio (WR) of calcium to potassium was unaffected. These results indicate that the iron metabolism is specifically affected in the *Nrf2*$^{-/-}$ mouse teeth.

General iron status in *Nrf2*$^{-/-}$ mice

To examine the reason why the iron metabolism of enamel organ was impaired in *Nrf2*$^{-/-}$ mice, we measured the general iron status in *Nrf2*$^{-/-}$ mice. We did not find any significant differences in haematocrit, serum iron concentration, total iron binding capacity (TIBC) and transferrin saturation (Table 2), indicating that the general iron status of *Nrf2*$^{-/-}$

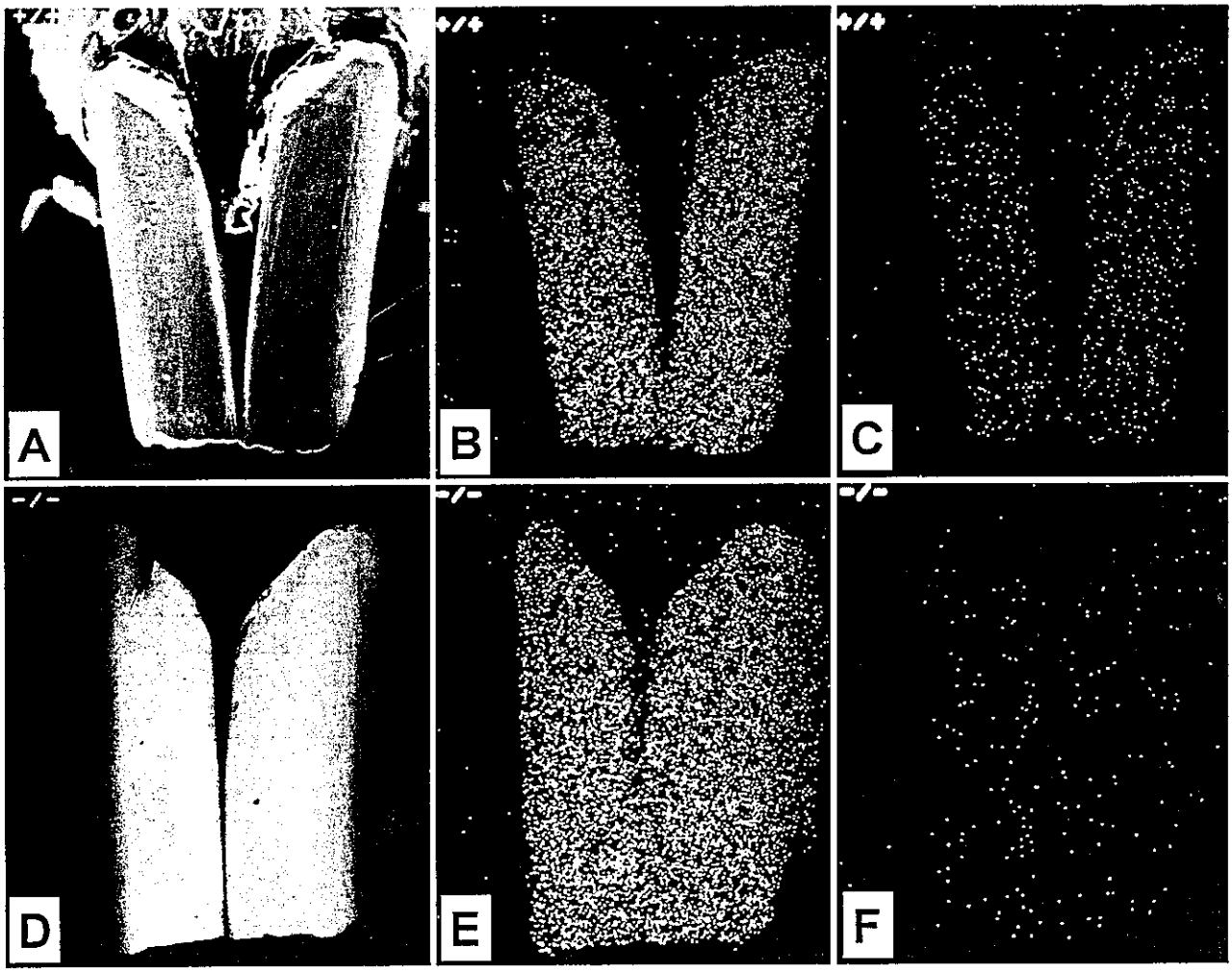

Figure 2 Scanning electron microscopic and micro X-ray analysis of the surface of the mouse incisor. (A, D) Scanning electron microscopic images of incisors of wild-type (A) and *Nrf2*$^{-/-}$ mouse (D). (B, E) Dot-map images of calcium on the surface of wild-type (B) and *Nrf2*$^{-/-}$ incisors (E) by micro X-ray analysis. (C, F) Dot-map images of iron on the surface of wild-type (C) and *Nrf2*$^{-/-}$ mouse incisors (F).

Table 1 Micro X-ray analysis of the incisors of *Nrf2*$^{-/-}$ mutant mice

	Nrf2 genotype		
	+/+	+/−	−/−
Fe percentage (w/w)	5.143 ± 0.754	2.748 ± 0.454*	0.396 ± 0.076*
Ca percentage (w/w)	36.389 ± 0.222	36.073 ± 0.039	36.161 ± 0.067
P percentage (w/w)	18.057 ± 0.091	17.808 ± 0.104	17.954 ± 0.047
Ca/P WR	2.016 ± 0.006	2.026 ± 0.011	2.015 ± 0.007
Ca/P MR	1.558 ± 0.005	1.566 ± 0.008	1.555 ± 0.007

The calcium, phosphorus, and iron contents of the enamel surface of wild-type, *Nrf2*$^{+/-}$, or *Nrf2*$^{-/-}$ incisors determined by micro X-ray analysis. The means from five incisors are presented with standard deviations. Student's *t*-test was used for the statistical analysis. *Significant difference compared with wild-type ($P < 0.001$). % (w/w), weigh percent; Ca/P WR, weight percentage ratio of calcium to phosphorus; Ca/P MR, molar ratio of calcium to phosphorus.

Table 2 General iron status of *Nrf2*$^{-/-}$ mice

	Nrf2 genotype	
	+/+	−/−
Hematocrit (%)	52.2 ± 4.9	52.7 ± 2.9
Serum iron (g/dL)	219.5 ± 40.6	271.0 ± 50.5
TIBC (g/dL)	407.8 ± 52.6	460.3 ± 71.2
Transferrin saturation (%)	54.4 ± 11.8	59.1 ± 8.7
Liver iron content (ng/mg)	55.5 ± 18.0	90.0 ± 11.7*

Hematocrit, serum iron concentration, total iron binding capacity (TIBC), transferrin saturation and liver iron content were measured in wild-type and Nrf2$^{-/-}$ mice. The means from six mice are presented with standard deviations. Mann–Whitney's *U*-test was used for the statistical analysis. *Significant difference compared with wild-type ($P < 0.01$).

mice is not affected. In contrast, non-haem iron content of liver was found to be significantly higher in *Nrf2*$^{-/-}$ mice than that in wild-type liver. The precise reason of this iron increase in the liver remains to be clarified.

Ameloblasts of *Nrf2*$^{-/-}$ mice show premature degenerative atrophy

We next examined development of ameloblasts in *Nrf2*$^{-/-}$ mouse, since it is the ameloblasts that deposit iron into the enamel surface. A histological examination with lower magnification of wild-type mouse tissues with haematoxylin and eosin staining showed slight signs of degenerative atrophy in the late maturation stage of the ameloblast development (lm, Fig. 3A). Compared to the wild-type mice, however, these changes in the *Nrf2*$^{-/-}$ mouse ameloblasts were abrupt and premature (below). We found that, while ameloblasts of *Nrf2*$^{-/-}$ mice showed very similar morphological appearance to that of the wild-type mice during the transition (t) stage and the early maturation (em) stage,

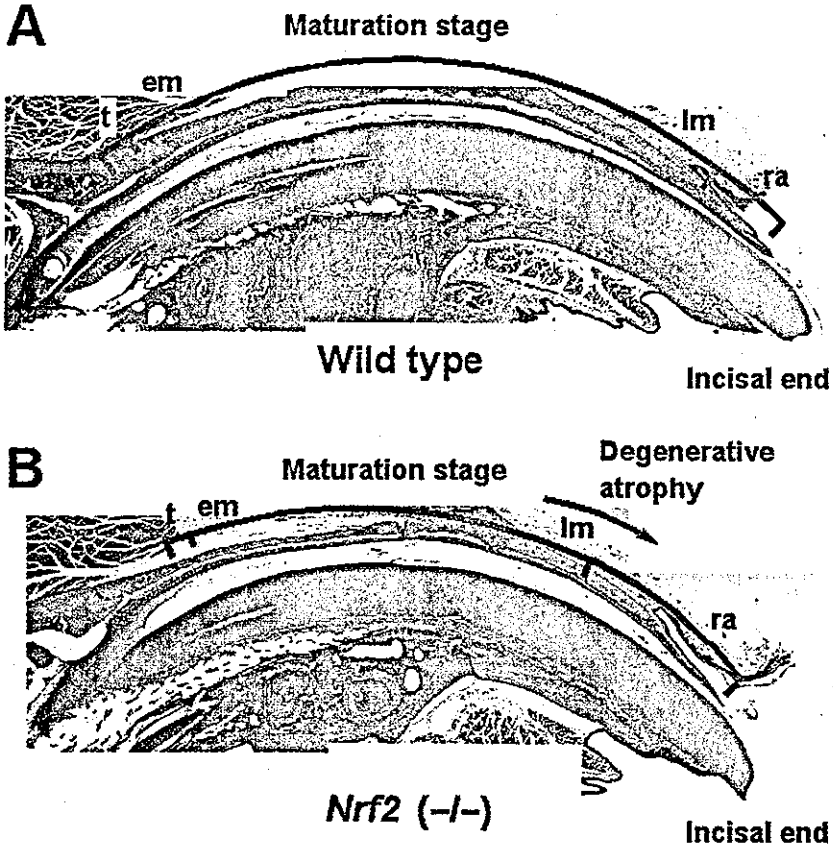

Figure 3 *Nrf2*$^{-/-}$ ameloblasts show degenerative atrophy at the late maturation stage. (A, B) Hematoxylin and eosin staining of wild-type (A) and *Nrf2*$^{-/-}$ (B) mouse enamel organs. The ameloblasts of *Nrf2*$^{-/-}$ mouse show severe premature degenerative atrophy at the late maturation stage (40 × original magnification). Abbreviations are: t, transition stage; em, early maturation stage; lm, late maturation stage; ra, region of reduced ameloblasts.

ameloblasts of *Nrf2*$^{-/-}$ mice suffered severely from premature degenerative atrophy at the late maturation stage (Fig. 3B; green arrow). The late maturation stage is the time when iron is excreted from ameloblasts to the enamel surface. At higher magnification, cell heights of ameloblasts gradually reduced from the early maturation stage to the late maturation stage in wild-type ameloblasts. At the stages of reduced ameloblasts, they were changed to atrophic flat squamous cells on the most incisal side. In agreement with the observations with the lower magnification sections (Fig. 3B), *Nrf2*$^{-/-}$ mice ameloblasts showed similar morphological appearance to the wild-type ameloblasts during the transition stage (Fig. 4A,C). However, the *Nrf2*$^{-/-}$ ameloblasts suffered from premature degenerative changes at the late maturation stage (Fig. 4D; compare with those in the wild-type mouse, Fig. 4B) and the flat squamous epithelia largely disappeared in the mutant mouse tissues (data not shown). These results thus demonstrate that the normal differentiation of ameloblasts are severely disturbed at the late maturation stage in the *Nrf2*$^{-/-}$ mice.

Iron transport is defective in *Nrf2*$^{-/-}$ mice

To examine whether the incomplete differentiation affects the ameloblasts function, iron metabolism during the ameloblast development was examined in *Nrf2*$^{-/-}$ mice. We carried out Berlin blue staining of wild-type and *Nrf2*$^{-/-}$ mouse incisors (Fig. 4, panels E–H). In the wild-type mouse incisors, positive staining of Berlin blue, which indicates the accumulation of iron, was detected in the ameloblast cytosol during the transition stage and early maturation stage (Fig. 4E). The accumulation of iron was then shifted to the plasma membrane on the enamel side at the late maturation stage, reflecting the iron excretion process into the enamel surface at this stage (Fig. 4F). No Berlin blue-positive staining was detected at the reduced ameloblast stage (data not shown). In the *Nrf2*$^{-/-}$ enamel organ, iron was detected both in the papillary layer cells and ameloblasts during the transition and early maturation stages, and the iron accumulation in the ameloblast cytosol was markedly decreased (Fig. 4G). This may be due to defect of the iron transport from blood vessels to the ameloblasts. We also found that the aberrant iron deposition overlapping with the degenerated cells (Fig. 4H), suggesting that the abnormal accumulation of iron might provoke, at least in part, the degeneration of papillary cells and ameloblasts of *Nrf2*$^{-/-}$ enamel organ.

Ferritin expression was decreased in *Nrf2*$^{-/-}$ papillary layer cells

Since ferritin is known to play an important role in the cellular iron metabolism, we next examined the expression of ferritin by immunohistochemical and *in situ* hybridization analyses. Ferritin heavy chain mRNA was expressed exclusively in the ameloblasts during transition and early maturation stages. The *Nrf2*$^{-/-}$ ameloblasts show similar level expression to the wild-type ameloblasts (Fig. 5C and 5A, respectively). However, ferritin heavy chain mRNA expression was very faint or not observed in the late maturation stage and reduced ameloblast stage (data not shown) of the ameloblast development in both wild-type and *Nrf2*$^{-/-}$ mice (Fig. 5B and 5D, respectively).

We also performed immunohistochemical analysis of ferritin expression, utilizing an anti-rat liver ferritin antibody that cross-reacts with mouse ferritin (Miyazaki *et al.* 1998). The analysis revealed that the expression level of ferritin protein was comparable between ameloblasts and papillary layer cells at the transition and early maturation stages in the wild-type mouse (Fig. 5E). Importantly, however, in the *Nrf2*$^{-/-}$ mouse the expression of ferritin in the papillary layer cells was significantly reduced compared to that in the ameloblasts (Fig. 5G). Consistent with the results of *in situ* ferritin heavy chain mRNA analysis, ferritin was expressed only faintly in the more advanced stages of ameloblasts (Fig. 5F,H). These results clearly indicate that although ferritin is expressed in the ameloblasts, it is not expressed efficiently in the papillary layer cells of *Nrf2*$^{-/-}$ animals (see Discussion).

Nrf2$^{-/-}$ teeth have decreased acid resistance

To assess changes in the quality of the teeth, we first examined the Knoop hardness of the teeth. However, we could not detect significant difference between wild-type and *Nrf2*$^{-/-}$ teeth. Therefore, we next examined acid resistance of *Nrf2*$^{-/-}$ teeth. For this purpose, the teeth were exposed to 0.1 M acetate buffer at pH 4.0 and amounts of eluted calcium ion were quantified at several time points by the methylxylenol blue method. As shown in Fig. 6, the concentration of eluted calcium ion from *Nrf2*$^{-/-}$ teeth was significantly higher than that from the wild-type teeth. The initial elution velocity increased rapidly, but the elution seems to be saturated at 30 and 40 min time points in *Nrf2*$^{-/-}$ teeth. The eluted calcium level from the *Nrf2*$^{-/-}$ teeth is significantly higher than that from the wild-type teeth ($P < 0.05$: Student's *t*-test). Thus, the acid resistance of *Nrf2*$^{-/-}$ teeth was significantly decreased compared to that of the wild-type mice, suggesting that the *Nrf2*$^{-/-}$ teeth are susceptible to dental caries.

Discussion

Closer examination of the *Nrf2*$^{-/-}$ mice unveiled that the surface colour of maxillary incisors of the *Nrf2*$^{-/-}$ mice is

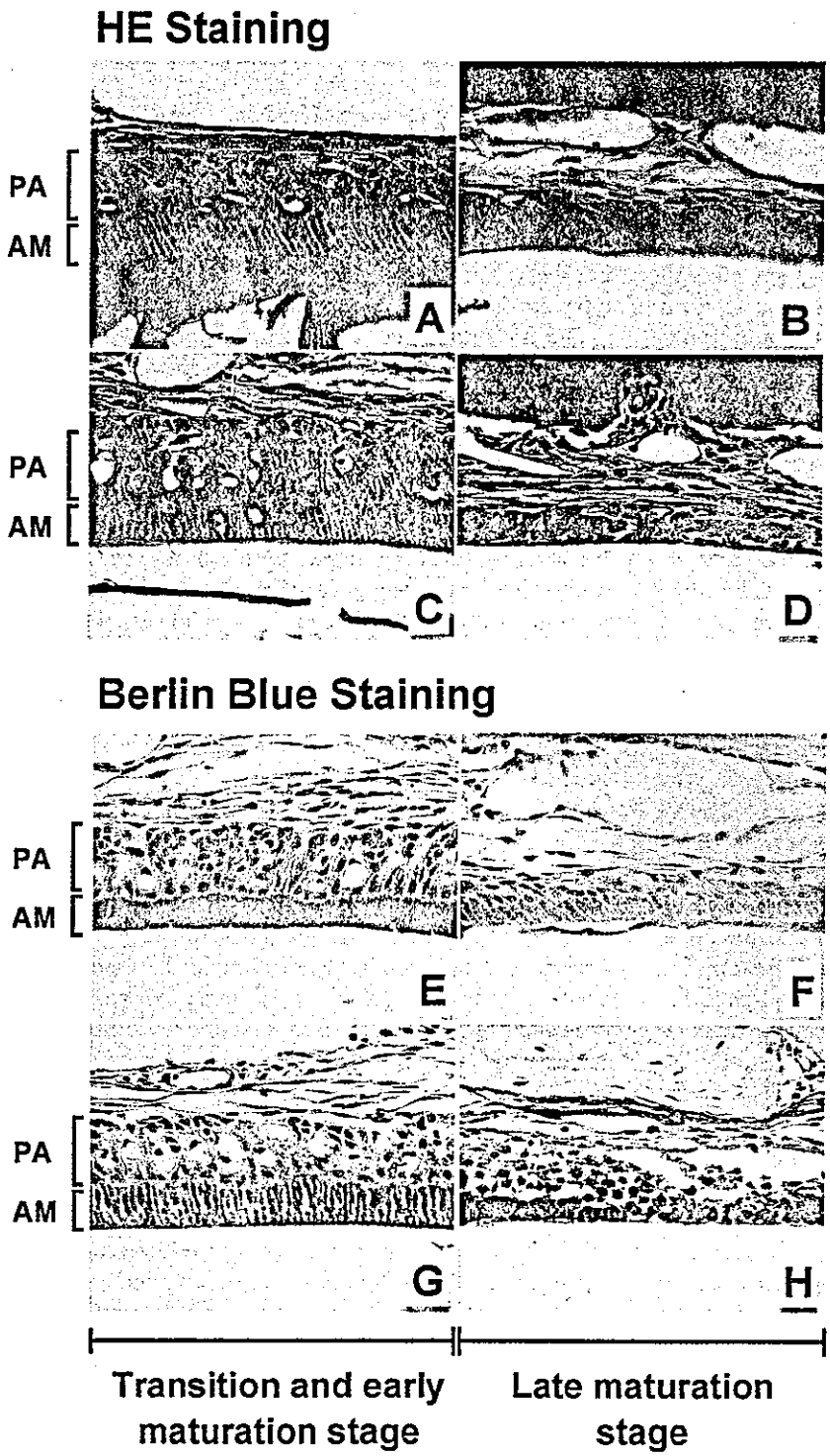

Figure 4 Defective iron transport in *Nrf2*$^{-/-}$ mouse enamel organ. (A–D) Hematoxylin and eosin staining of wild-type (A, B) and *Nrf2*$^{-/-}$ (C, D) mouse enamel organs. (E–H) Berlin blue staining of wild-type (E, F) and *Nrf2*$^{-/-}$ (G, H) mouse enamel organs. (A, C, E, G) show the transition stage, while (B, D, F, H) show the late maturation stage of ameloblast maturation. AM, ameloblasts; PA, Papillary cell layer.

greyish white, which is a marked contrast to the yellowish brown colour of the wild-type mouse incisors. Our analyses further revealed that this decolourization is due to the decrease in the iron content of the mature enamel.

The analysis of iron metabolism in the enamel organ showed that the iron transport from blood vessels to the ameloblasts was disturbed in the *Nrf2*$^{-/-}$ mouse during the ameloblast maturation stages. In the *Nrf2*$^{-/-}$ mouse,

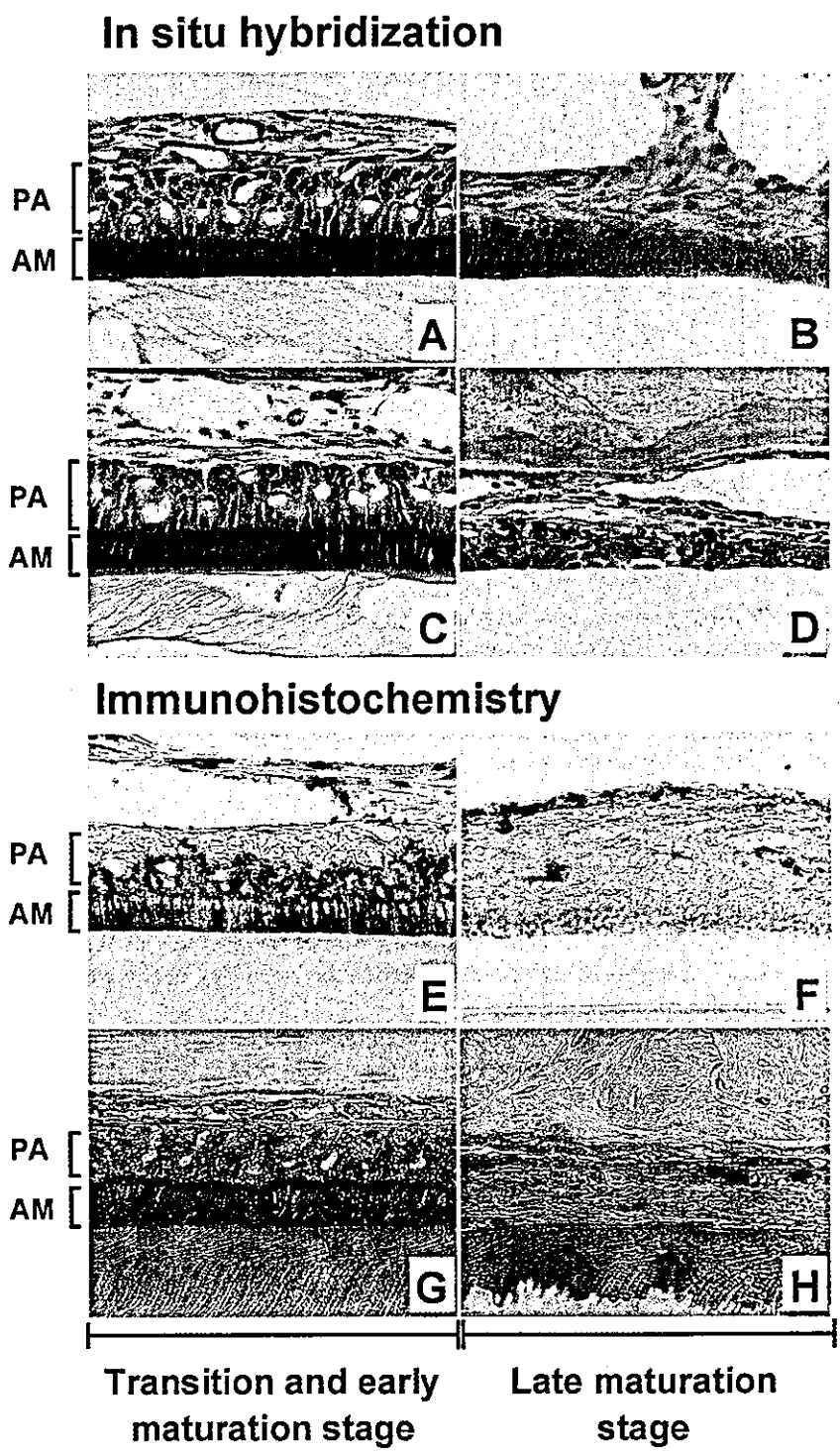

Figure 5 Expression of ferritin and ferritin heavy chain mRNA in *Nrf2*$^{-/-}$ enamel organ. (A–D) *In situ* hybridization analysis of ferritin heavy chain mRNA of wild-type (A, B) and *Nrf2*$^{-/-}$ (C, D) mouse enamel organs. (E–H) Immunohistochemical analysis of ferritin in the wild-type (E, F) and *Nrf2*$^{-/-}$ (G, H) mouse enamel organs. (A, C, E, G) show the transition stage, while (B, D, F, H) show the late maturation stage of ameloblast maturation. AM, ameloblasts; PA, Papillary cell layer.

ameloblasts underwent severe degenerative changes and disappeared prematurely during their maturation stages, so the loss of the ameloblast function resulted in the failure of iron deposition to the enamel surface and the decolourization of the incisors. To our knowledge, this is the first report describing the iron metabolism disorder in the *Nrf2*$^{-/-}$ mouse.

Iron is critically involved in various cellular events ranging from DNA synthesis to cellular respiration (Cammack *et al.* 1990). Among them, the iron utilization

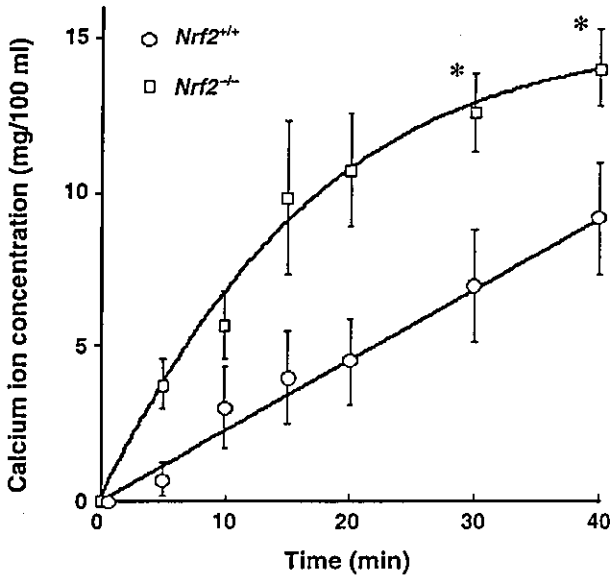

Figure 6 *Nrf2*$^{-/-}$ mice incisors have diminished acid resistance. A 0.5 mm × 5 mm area of the buccal surface of murine incisors was exposed to acetate buffer at pH 4.0, and the amount of eluted calcium ion was determined. The surface of the *Nrf2*$^{-/-}$ tooth (□) eroded significantly earlier in acetic acid than that of the wild-type mice (○). *$P < 0.05$: Student's t-test.

in the rodent enamel organ illustrates one of the most interesting examples of iron usage in mammals. Iron deposited on to the enamel surface seems to contribute to the formation of acid resistance and hardness of the rodent incisors, which is advantageous for grinding the hard seeds in the environment (Halse 1974; Stein & Boyle 1959). In fact, the diminished acid resistance of iron-poor *Nrf2*$^{-/-}$ teeth (Fig. 6) supports the notion that the iron deposition in the enamel surface is an important event to preserve the rodent tooth function.

In terms of the iron and calcium transport, as well as matrix and water removal, the papillary layer cells have been shown to form an intimate functional unit with the ameloblasts during early to late stages of the enamel maturation (Ohshima *et al.* 1998; Garant & Gillespie 1969; Skobe & Garant 1974). Importantly, transferrin receptors are found to be mainly expressed in the papillary layer cells of the enamel organ of rat incisors (Mataki *et al.* 1989), suggesting that the papillary layer cells uptake iron efficiently from the circulating blood. Although mechanism of the next transfer process of iron, i.e. from the papillary layer cells to ameloblasts, is not well understood at present, one plausible explanation for this is that the transferrin-bound iron from the circulating blood may be transferred to ferritin within the papillary layer cells, and subsequently the ferritin-bound iron is transferred to ameloblasts. Consistent with this contention, we observed high ferritin protein accumulation both in the ameloblasts and papillary layer cells in the wild-type enamel organ.

Ferritin serves as the transient iron reservoir in mature ameloblasts, and surprisingly the ameloblasts express ferritin mRNA most abundantly amongst rat tissues (Miyazaki *et al.* 1998). Ferritin is a 480-kDa intracellular protein that can store up to 4500 atoms of iron. The protein consists of heavy and light chains. The ratio of subunits within a ferritin molecule varies widely from tissue to tissue, which in turn modulates the ferritin function (Miyazaki *et al.* 1998). Although ferritin is expressed at equal levels both in ameloblasts and papillary layer cells in the wild-type enamel organ, the *in situ* analysis of ferritin heavy chain mRNA expression demonstrates that the mRNA is exclusively expressed in the ameloblasts. This observation suggests that the ferritin synthesized in the ameloblasts may be transferred to the papillary cells (Mataki *et al.* 1989). An alternative, and less likely, possibility is that the expression of ferritin mRNA in papillary cells might be under the detection limit of the *in situ* hybridization method and efficient translation compensated for the weak expression of the gene at mRNA level.

While ferritin is abundantly accumulated, iron accumulation is scarcely observed in the papillary layer cells of the wild-type mouse. This observation suggests that the iron transfer process from the papillary layer cells to ameloblasts may be very efficient in the wild-type enamel organ. We envisage that ferritin may be loaded with iron in the papillary layer cells and rapidly transferred to the ameloblasts.

An important observation is that the accumulation level of ferritin is abnormally reduced, but accumulation level of iron is abnormally increased, in the *Nrf2*$^{-/-}$ papillary layer cells, suggesting that the iron transfer process is somehow disturbed in the *Nrf2*$^{-/-}$ enamel organ. We envisage the following scenario to explain the observation, which is depicted schematically in Fig. 7. Since the expression levels of ferritin heavy chain mRNA and ferritin protein in the *Nrf2*$^{-/-}$ ameloblasts was almost comparable to those of the wild-type ameloblasts (see Fig. 5), a translocation or recycling step of ferritin from the ameloblasts to the papillary layer cells might be affected in the *Nrf2*$^{-/-}$ mice (Radisky & Kaplan 1998; Kwok & Richardson 2003). Although the translocation of ferritin from ameloblasts to papillary layer cells has not been evidenced to date, such a mechanism might be affected in *Nrf2*$^{-/-}$ enamel organ most probably because of the enhanced oxidative stress in ameloblasts.

An alternative explanation is that the decrease in the ferritin mRNA expression may be involved in the

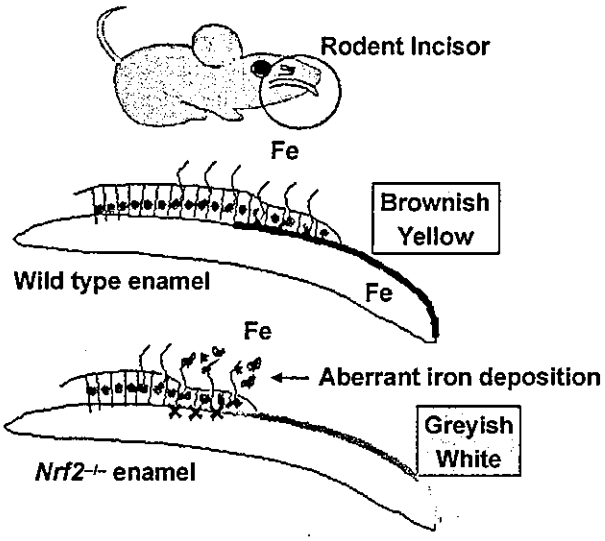

Figure 7 *Nrf2*$^{-/-}$ mice were defective in iron utilization in developing enamel organ. *Nrf2*$^{-/-}$ teeth were greyish white (bottom panel), whereas those of wild-type mice were brownish yellow (middle panel). This decolourization is owing to the defect of iron deposition in the mature enamel surface. *Nrf2*$^{-/-}$ enamel organs have iron transport defect that leads to both enamel cell degeneration and disturbed iron deposition orf to the enamel surface. Brown arrows designate the direction of iron transport and subsequent deposition.

decrease of ferritin in the *Nrf2*$^{-/-}$ papillary cells. Indeed, it was recently reported that the chemical activators of Nrf2 up-regulates the ferritin heavy and light chain gene expression *in vivo*, indicating that the ferritin gene expression is under the regulation of Nrf2/ARE pathway (Primiano *et al.* 1996; Tsuji *et al.* 2000; Pietsch *et al.* 2003). Supporting this contention, it was also reported that the expression of ferritin genes is not induced, but basal level of the gene expression is rather reduced in *Nrf2*$^{-/-}$ mouse embryonic fibroblasts (Pietsch *et al.* 2003). Moreover, decrease in the basal expression as well as the induction of ferritin gene was found in *Nrf2*$^{-/-}$ astrocytes (Lee *et al.* 2003). The basal level expression of ferritin mRNA in *Nrf2*$^{-/-}$ small intestine was also decreased in a microarray analysis (Thimmulappa *et al.* 2002). Thus, further analyses is required to clarify the underlying mechanisms of iron transport defect observed in *Nrf2*$^{-/-}$ enamel organ.

The aberrant accumulation of iron in *Nrf2*$^{-/-}$ papillary cells seems to lead the ameloblasts to premature degeneration by oxidative stress, as iron generates highly reactive oxygen species via Fenton chemistry and causes an oxidative stress to cells (Linn 1998). Upon utilization of iron therefore cells need to be equipped with an array of anti-oxidant systems to prevent its toxicity. Since Nrf2 regulates expression of the genes that protect cells from oxidative stress (Ishii *et al.* 2000; Itoh *et al.* 1999b), there is a possibility that defective expression of certain Nrf2/ARE-regulated gene(s) might be involved in the degenerative changes observed in the *Nrf2*$^{-/-}$ enamel organ. For the understanding of the iron transport system that is defective in the *Nrf2*$^{-/-}$ mouse, comprehensive as well as quantitative analyses of the expression of ARE-regulated genes in the enamel organ is critically important. However, we need a technical breakthrough for collecting enough amounts of mouse enamel organs for such analyses.

Experimental procedures

Macroscopic observation

The generation of *Nrf2* gene mutant mice was previously described (Itoh *et al.* 1997). The incidence of decolourization phenotype was analysed by the χ^2-test.

Scanning electron microscopic observation and micro X-ray analysis

The murine incisors, including maxillary bones, were fixed in 100% ethanol and dehydrated by the critical point drying method. The incisors from *Nrf2*$^{+/-}$ and *Nrf2*$^{-/-}$ mice were examined using a scanning electron microscope (Hitachi S-2500CX) operated at 15 kV. Micro X-ray analysis was performed to determine the chemical components of the incisors. For energy-dispersive X-ray analysis, an X-ray detector system (Kevex Quantum Delta IV) attached to a scanning electron microscope was used. The micro X-ray analysis system was operated at a 15-kV accelerating voltage and a 0.1-nA probe current, with a 20-nm probe size and a 100-s counting time. Five points on the enamel surface were selected and analysed for the amounts of calcium, phosphorus and iron. The iron concentration was detected in 1 μm depth of enamel surface.

In situ hybridization, immunohistochemistry and iron staining

Ferritin heavy chain cDNA was subcloned into the pBluescript KS$^+$ vector and used as a template for cRNA production. DIG-11-UTP-labelled single-strand anti-sense and sense RNA probes were prepared by DIG-RNA Labeling Kit (Behringer Mannheim) according to the manufacturer's instruction. Samples were fixed with 4% paraformaldehyde with PBS overnight at 4 °C and decalcified in 10% EDTA (pH 7.4) for 2 weeks, embedded in paraffin and sectioned. *In situ* hybridization was performed as previously described (Shibata *et al.* 2000). After treatment with 0.2 N hydrochloric acid and Proteinase K (10 μg/mL), hybridization was performed with the probe (1 μg/mL) at 50 °C overnight. After extensive washing and RNase A treatment, the hybridized DIG-labelled probes were detected with alkaline phosphatase-

conjugated anti-DIG antibody and 5-bromo-4-chloro-3-indolyl phosphate as the substrate, using a nucleic acid detection kit (Behringer Manheim).

Immunostaining was performed using the labelled streptavidin biotin method (LsAB method: Nichirei). Sections were immersed in 0.3% hydrogen peroxide in methanol for 30 min, and incubated with 5% normal goat serum for 30 min at room temperature. The sections were then incubated with anti-rat liver ferritin rabbit polyclonal antibody (1 : 200 v/v) in PBS at 4 °C overnight (Miyazaki *et al.* 1998). The slides were reacted with biotinylated goat anti-rabbit antibody for 30 min at room temperature, followed by horseradish peroxidase conjugated with streptavidin. The peroxidase activity was visualized by the 3-amino-9-ethylcarbasol substrate-chromogen system (Nichirei, Tokyo). The sections were counterstained with haematoxylin, dehydrated, and mounted. Control staining was performed with non-immune rabbit serum. Berlin blue staining was performed to detect iron deposits.

Serum iron parameters and liver iron content

Blood was obtained from abdominal aorta of anaesthetized mice and 200 μL of serum from each animal was used for analysis of iron and total iron binding capacity. These assays were performed by SRL Inc. (Tokyo) using an automatic chemical analyser (Hitachi). Non-haem iron in the liver was measured as previously described (Foy *et al.* 1967).

Analysis of acid resistance and Knoop hardness

Hardness test of the enamel surface was performed by using a hardness tester equipped with a Knoop penetrator. Six kg load was applied to each tooth for 10 s. To measure the acid resistance of the teeth, a 5 mm × 0.5 mm of the buccal surface of the murine incisors was exposed to 100 μL of acetate buffer (100 mM) at pH 4.0 at room temperature. The eluted calcium ion was measured by the methylxylenol blue method (Calcium *E*-test Wako, Wako, USA) at 5, 10, 15, 20, 30 and 40 min. The means from five independent incisors from 8 to 12-week-old mice were presented with standard errors.

Acknowledgements

We thank Dr Takanobu Isokawa and *Kitl*. Tong for discussion and advice. This work was supported in part by grants from JST-ERATO, JSPS, the Ministry of Education, Culture, Sports, Science and Technology, the Ministry of Health, Labor and Welfare, CREST, and the Naito foundation.

References

Aoki, Y., Sato, H., Nishimura, N., Takahashi, S., Itoh, K. & Yamamoto, M. (2001) Accelerated DNA adduct formation in the lung of the Nrf2 knockout mouse exposed to diesel exhaust. *Toxicol. Appl. Pharmacol.* **173**, 154–160.

Cammack, R., Wriggleworth, J.M. & Baum, H. (1990) Iron dependent enzymes in mammalian systems. In: *Iron Transport and Storage* (eds P. Ponka, H. M. Schulman & R. C. Woodworth), pp. 17–40. Boca Raton: CRC Press.

Chan, K., Han, X.D. & Kan, Y.W. (2001) An important function of Nrf2 in combating oxidative stress: detoxification of acetaminophen. *Proc. Natl. Acad. Sci. USA* **98**, 4611–4616.

Chan, K. & Kan, Y.W. (1999) Nrf2 is essential for protection against acute pulmonary injury in mice. *Proc. Natl. Acad. Sci. USA* **96**, 12731–12736.

Cho, H.Y., Jedlicka, A.E., Reddy, S.P., *et al.* (2002) Role of NRF2 in Protection Against Hyperoxic Lung Injury in Mice. *Am. J. Respir. Cell. Mol. Biol.* **26**, 175–182.

Enomoto, A., Itoh, K., Nagayoshi, E., *et al.* (2001) High sensitivity of Nrf2 knockout mice to acetaminophen hepatotoxicity associated with decreased expression of ARE-regulated drug metabolizing enzymes and antioxidant genes. *Toxicol. Sci.* **59**, 169–177.

Foy, A.L., Williams, H.L., Cortell, S. & Conrad, M.E. (1967) A modified procedure for the determination of non-heme iron in tissue. *Anal. Biochem.* **18**, 559–563.

Garant, P.R. & Gillespie, R. (1969) The presence of fenestrated capillaries in the papillary layer of the enamel organ. *Anat. Rec.* **163**, 71–79.

Halse, A. (1973) Effect of dietary iron deficiency on the pigmentation and iron content of rat incisor enamel. *Scand. J. Dent. Res.* **81**, 319–334.

Halse, A. (1974) Electron microprobe analysis of iron content of incisor enamel in some species of Rodentia. *Arch. Oral. Biol.* **19**, 7–11.

Halse, A. & Selvig, K.A. (1974) Incorporation of iron in rat incisor enamel. *Scand. J. Dent. Res.* **82**, 47–56.

Ishii, T., Itoh, K., Takahashi, S., *et al.* (2000) Transcription factor Nrf2 coordinately regulates a group of oxidative stress-inducible genes in macrophages. *J. Biol. Chem.* **275**, 16023–16029.

Itoh, K., Chiba, T., Takahashi, S., *et al.* (1997) An Nrf2/small maf heterodimer mediates the induction of phase II detoxifying enzyme genes through antioxidant responsive element. *Biochem. Biophys. Res. Commun.* **236**, 313–322.

Itoh, K., Igarashi, K., Hayashi, N., Nishizawa, M. & Yamamoto, M. (1995) Cloning and characterization of a novel erythroid cell-derived CNC family transcription factor heterodimerizing with the small maf family proteins. *Mol. Cell. Biol.* **15**, 4184–4193.

Itoh, K., Ishii, T., Wakabayashi, N. & Yamamoto, M. (1999a) Regulatory mechanisms of cellular response to oxidative stress. *Free Radic. Res.* **31**, 319–324.

Itoh, K., Wakabayashi, N., Katoh, Y., *et al.* (1999b) Keap1 represses nuclear activation of antioxidant responsive elements by Nrf2 through binding to the amino-terminal Neh2 domain. *Genes Dev.* **13**, 76–86.

Kallenbach, E. (1970) Fine structure of rat incisor enamel organ during late pigmentation and regression stages. *J. Ultrastruct. Res.* **30**, 38–63.

Karim, A. & Warshawsky, H. (1984) A radioautographic study of the incorporation of iron 55 by the ameloblasts in the zone of maturation of rat incisors. *Am. J. Anat.* **169**, 327–335.

Kuroha, T., Takahashi, S., Komeno, T., Itoh, K., Nagasawa, T. & Yamamoto, M. (1998) Ablation of Nrf2 function does not

increase the erythroid or megakaryocytic cell lineage dysfunction caused by p45 NF-E2 gene disruption. *J. Biochem.* **123**, 376–379.

Kwok, J.C. & Richardson, D.R. (2003) Anthracyclines induce accumulation of iron in ferritin in myocardial and neoplastic cells: inhibition of the ferritin iron mobilization pathway. *Mol. Pharmacol.* **63**, 849–861.

Lee, J.M., Calkins, M.J., Chan, K., Kan, Y.W. & Johnson, J.A. (2003) Identification of the NF-E2-related factor-2-dependent genes conferring protection against oxidative stress in primary cortical astrocytes using oligonucleotide microarray analysis. *J. Biol. Chem.* **278**, 12029–12038.

Linn, S. (1998) DNA damage by iron and hydrogen peroxide in vitro and in vivo. *Drug Metab. Rev.* **30**, 313–326.

Mataki, S., Ohya, M., Kubota, M., Ino, M. & Ogura, H. (1989) Immunohistochemical and pharmacological studies on the distribution of ferritin and its secretory process of amelolasts in rat incisor enamel. In: *Tooth Enamel* (ed. R. W. Fearnhead), pp. 108–112. Yokohama: Yokohama Florence Publishers.

McCord, J.M. (1998) Iron, free radicals, and oxidative injury. *Semin. Hematol.* **35**, 5–12.

Miyazaki, Y., Sakai, H., Shibata, Y., Shibata, M., Mataki, S. & Kato, Y. (1998) Expression and localization of ferritin mRNA in ameloblasts of rat incisor. *Arch. Oral. Biol.* **43**, 367–378.

Mohler, J., Vani, K., Leung, S. & Epstein, A. (1991) Segmentally restricted, cephalic expression of a leucine zipper gene during Drosophila embryogenesis. *Mech. Dev.* **34**, 3–9.

Ohshima, H., Maeda, T. & Takano, Y. (1998) Cytochrome oxidase activity in the enamel organ during amelogenesis in rat incisors. *Anat. Rec.* **252**, 519–531.

Pietsch, E.C., Chan, J.Y., Torti, F.M. & Torti, S.V. (2003) Nrf2 mediates the induction of ferritin H in response to xenobiotics and cancer chemopreventive dithiolethiones. *J. Biol. Chem.* **278**, 2361–2369.

Primiano, T., Kensler, T.W., Kuppusamy, P., Zweier, J.L. & Sutter, T.R. (1996) Induction of hepatic heme oxygenase-1 and ferritin in rats by cancer chemopreventive dithiolethiones. *Carcinogenesis.* **17**, 2291–2296.

Radisky, D.C. & Kaplan, J. (1998) Iron in cytosolic ferritin can be recycled through lysosomal degradation in human fibroblasts. *Biochem. J.* **336**, 201–215.

Ramos-Gomez, M., Kwak, M.K., Dolan, P.M., *et al.* (2001) Sensitivity to carcinogenesis is increased and chemoprotective efficacy of enzyme inducers is lost in nrf2 transcription factor-deficient mice. *Proc. Natl. Acad. Sci. USA* **98**, 3410–3415.

Shibata, Y., Fujita, S., Takahashi, H., Yamaguchi, A. & Koji, T. (2000) Assessment of decalcifying protocols for detection of specific RNA by non-radioactive in situ hybridization in calcified tissues. *Histochem. Cell Biol.* **113**, 153–159.

Skobe, Z. & Garant, P.R. (1974) Electron microscopy of horseradish peroxidase uptake by papillary cells of the mouse incisor enamel organ. *Arch. Oral. Biol.* **19**, 387–395.

Stein, G. & Boyle, P.E. (1959) Pigmentation of the enamel of albino rat incisor teeth. *Arch. Oral Biol.* **1**, 97–105.

Takano, Y. & Ozawa, H. (1981) Cytochemical studies on the ferritin-containing vesicles of the rat incisor ameloblasts with special reference to the acid phosphatase activity. *Calcif. Tissue Int.* **33**, 51–55.

Thimmulappa, R.K., Mai, K.H., Srisuma, S., Kensler, T.W., Yamamoto, M. & Biswal, S. (2002) Identification of Nrf2-regulated genes induced by the chemopreventive agent sulforaphane by oligonucleotide microarray. *Cancer Res.* **62**, 5196–5203.

Tsuji, Y., Ayaki, H., Whitman, S.P., Morrow, C.S., Torti, S.V. & Torti, F.M. (2000) Coordinate transcriptional and translational regulation of ferritin in response to oxidative stress. *Mol. Cell. Biol.* **20**, 5818–5827.

Yoh, K., Itoh, K., Enomoto, A., *et al.* (2001) Nrf2 deficient female mice develop lupus-like autoimmune nephritis. *Kidney Int.* **60**, 1343–1353.

Received: 10 January 2004
Accepted: 13 April 2004